

# State of art simulation of climatic circulation in the Indian Ocean

## 4.1 Introduction

The Indian Ocean is an ideal place to study the time-dependent response of the ocean to changing winds. The time-dependent evolution of circulation at various levels in the Indian Ocean and its underlying mechanisms are poorly understood. Better understanding of the ocean dynamics can be achieved only by using state of art simulation models. As mentioned in Chapter-II and Chapter-III, the diagnostic and semi-diagnostic circulation models yield steady state circulation of the ocean taking into consideration only the local forcing of wind changes and the internal density field. The time-varying circulation of the Indian Ocean is controlled by both the local forcing and remote forcing by long waves. Long waves (Le Bland et al., 1980) comprise mainly three types, mainly the westward propagating Rossby waves (period 50-180 days) and Yanai waves (period 25 days) and eastward propagating Kelvin waves (period 50-180 days). The Kelvin waves propagate eastwards with the coast on the right side in the northern hemisphere. It is regarded as a coastally trapped wave within a certain distance from the coast, because its amplitude decays outside that distance so as to be hardly discernible. Along the equator, the coriolis force is zero and hence the equator also serves as a wave-guide. An equatorial Kelvin wave may be thought as two parallel coastal Kelvin waves propagating with the boundary on the right in the northern hemisphere and left in the southern hemisphere. As a result, Kelvin waves can propagate eastwards along the equator. The Rossby waves are large scale dynamical response of the ocean to wind forcing at the eastern boundaries and the ocean interior. They can also be generated by perturbation along the eastern boundaries associated with coastally trapped waves originating at low latitudes.

## **4.2 Features of sigma coordinate simulation model of circulation**

The main goal of this chapter is to study the large scale, time-dependent, 3-dimensional circulation of the Indian Ocean and to understand the dynamical mechanisms which are responsible for the observed circulation. The governing equations of the state of art ocean circulation model are the primitive equations of motion in spherical sigma co-ordinates, with hydrostatic, boussinesq and rigid lid approximations. Details of these equations are given in Chapter-II. In the prognostic mode, the basic equations as given in Chapter-II (equations 2.15-2.21 together with the equations for stream function 2.26) remain the same; however, the surface boundary conditions in prognostic mode differ from that used in diagnostic and semi-diagnostic modes. The fundamental changes in the surface boundary conditions are that all the surface boundary conditions such as wind stress, heat and salt fluxes are to be interpolated at each time step of model integration. In the diagnostic and semi-diagnostic modes, the surface boundary conditions for wind stress, temperature and salinity were constant in time throughout the model integration, and the density field is not evolved in time; the density field is imposed on the model from observations of temperature and salinity. The heat and salt flux surface boundary conditions are not used in diagnostic or semi-diagnostic mode. All the other features and parameters of the simulation model and semi-diagnostic model are the same, and these details are already given in section 2.2.3. The boundary conditions for the lateral (rigid) and bottom are given by equations 2.23 and 2.24. The model has two liquid boundaries at 36°S and 142°E. On the liquid boundaries, zero flux condition is set for velocity fields; the temperature and salinity data (Levitus, et al., 1994) at the liquid boundaries are interpolated at each time step of model integration and prescribed at the southern and eastern liquid boundaries. In this version of the model, the run-off from rivers Brahmaputra, Ganges and Indus that contributes considerably to the salinity distribution are taken into account, and this is done in a simple way; time-dependent boundary conditions for velocity, temperature and

salinity fields were prescribed at the model grid points situated along the river discharge boundary; in the regions where the above mentioned rivers enter, the temperature and salinity data across the entire depth at the boundary were first extracted from Levitus database and then interpolated at each time step of model integration. From the river discharge data (UNESCO, 1969), the velocity fields at the model grid points along the river discharge boundary for all the 12 months were calculated and interpolated at each time step of model integration.

Monthly mean meteorological fields derived from National Centre for Environmental Prediction/National Centre for Climate Research (NCEP/NCAR) reanalysis data (Kalnay et al., 1996) were used to calculate wind stress, heat and salt fluxes which are the surface boundary conditions for the simulation model. These monthly mean climatic data sets were averaged over the period 1982-1994 and then used as surface boundary condition. The methodology for the calculation of wind stress, heat and salt fluxes were given in sections 2.3.1 to 2.3.3 of Chapter-II. These monthly mean data were subsequently interpolated at each time step of model integration by using the formula 2.33 and 2.34.

Like the semi-diagnostic model, the simulation model has been adapted and configured to the Indian Ocean area between the latitude belt 36°S-29.5°N and longitude belt 22°E – 142°E, with a resolution of 1° x 0.5° in the longitude and latitude directions respectively. It has 33 levels in the vertical at standard oceanographic depths. The model was initialized with temperature and salinity 3-D fields from January Levitus climatology (1994). Linear interpolation was used for interpolating 3-D temperature and salinity fields from z to sigma co-ordinate. The model initial conditions for velocity fields are a state of rest ( $u = v = w = 0$ ). The model was integrated forward with a time step of 3 hours for 10 years using the surface climatological forcing which are applied with cyclic condition in time. From the analysis of the computed results, it was found that the

solution attained equilibrium by the 10<sup>th</sup> year of simulation. Thus, the 10<sup>th</sup> year of simulation was selected for the interpretation of model climate. The mid-month fields of the 10<sup>th</sup> year simulation were compared with existing observations and with results from SODA ( Simple Ocean Data Assimilation). SODA is an application of data assimilation using a forecast model based on GFDL (Carton et al., 2000).

### **4.3 Forcing parameters**

As mentioned in the previous section, the state of art simulation model is forced with climatological wind stress derived from NCEP reanalysis. The methodology for the computation of net heat and fresh water flux and a brief description of all these forcing fields for selected months except heat and fresh water fluxes were presented in Chapter –III. Briefly given below the distribution of net heat and fresh water fluxes (P-E) for the months of January, April, July and October (Fig. 4.1 and 4.2). Negative values in the figures indicate that heat is lost from the ocean and positive values denote gain by the ocean.

#### **(a) Net heat balance**

During January, net heat flux is negative in the northern Indian Ocean and is positive in the southern Indian Ocean. The maximum heat loss of 75 W/m<sup>2</sup> is observed in the central Arabian Sea. January being southern summer, more insolation is received over the southern Indian Ocean. The maximum values are observed in the regions south of 15°S.

During the month of April, the net heat flux is positive over the Arabian Sea and Bay of Bengal where as it is negative in the southern tropical Indian Ocean. Maximum insolation is received in the Bay of Bengal and Arabian Sea during April.

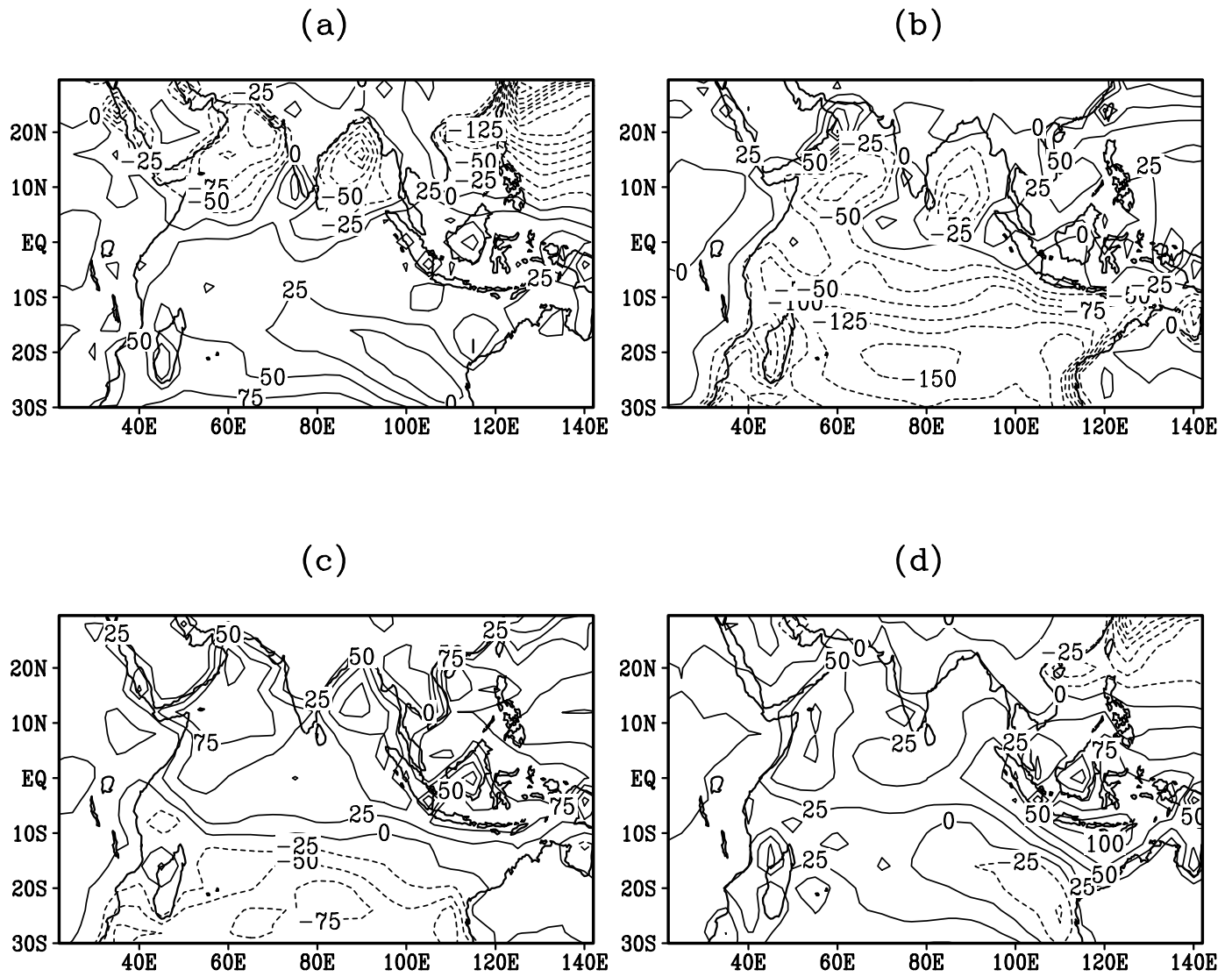


Fig.4.1. Spatial distribution of net heat flux ( $W/m^2$ ) for different months

(a) January (b) July (c) April (d) October

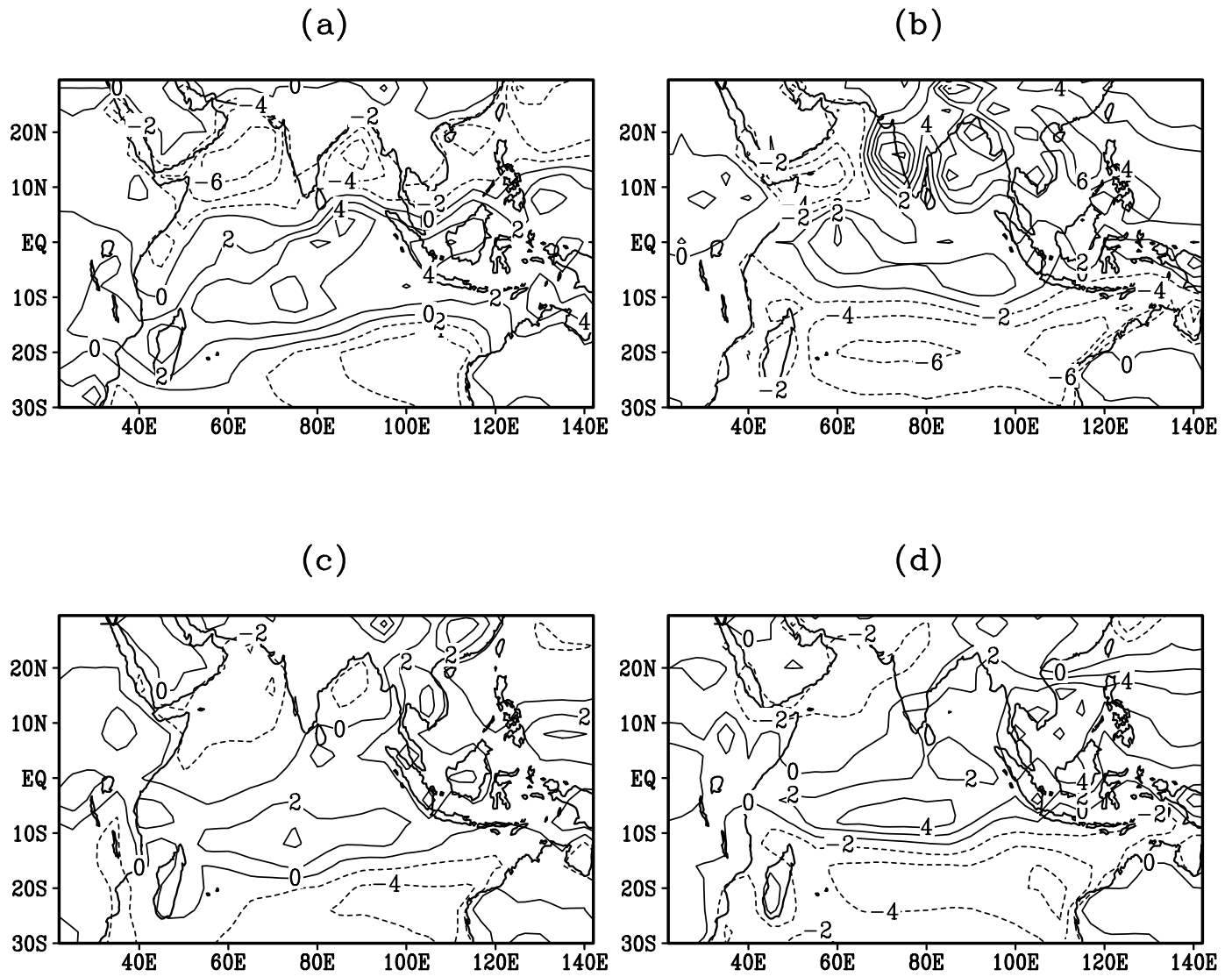


Fig.4.2. Difference between precipitation and evaporation (P-E) in (mm/day) for different months. (a) January (b) July (c) April (d) October

During July, the net heat flux is negative throughout the tropical Indian Ocean including Bay of Bengal and Arabian Sea. This is due to heavy evaporation in the summer season. By October, the heat flux is again positive throughout the tropical Indian Ocean due to excess insolation. As the wind is weak during the transition month of October, there is less evaporative heat loss and hence the net heat flux is positive.

#### **(b) Fresh water flux**

During January, the (P-E) term is positive in the equatorial regions. January is the time when the ITCZ is just south of the equator. This gives more precipitation in the equatorial band and hence (P-E) term is positive. In the northern Indian Ocean, and south of 15°S, evaporation is excess over precipitation and hence the (P-E) term is negative.

In April, equatorial regions are characterised by positive (P-E) indicating excess precipitation over evaporation. During July, the regions north of 10°S is under the influence of southwesterly monsoon winds and there is heavy rainfall. Hence (P-E) term is positive in the equatorial belt; however, (P-E) term is negative in the western Arabian Sea because of excess evaporation over precipitation during the monsoon months. Over the subtropical high pressure zone, (P-E) is negative due to excess evaporation.

### **4.4 Model circulation and comparison with observations / models :**

#### **4.4.1 Model circulation in the tropical Indian Ocean during various seasons**

There are very limited observations on currents at the subsurface levels of Indian Ocean and hence the only reliable way to validate our model results will be to compare the results with other state of art simulation model which were used for the simulation of Indian Ocean circulation. In this chapter, the circulation model results were compared with the circulation

from the SODA database. The volume transport of the major current systems in the Indian Ocean were also computed and compared with available observations. The volume transport is computed by taking the depth integral of the meridional extent of the zonal current along a longitudinal section and the zonal extent of the meridional current along a latitudinal section.

#### **(a) Circulation during January**

In the northern Indian Ocean, the surface circulation during January is dominated by the presence of NMC (North East Monsoon Current) flowing westward from the equator to 5°N with an average speed of 50cm/s (Fig. 4.3). The simulation model NMC is weaker as compared to SODA NMC. This zonal current splits at the coast near 4°N to two alongshore flows; one branch flows southward, which is known as winter Somali Current (SC) and the other branch flows northward. The southward flowing winter Somali Current meets the East African Coastal Current (EACC) near 2°S, where both of them turn offshore to form the South Equatorial Counter Current (SECC) in agreement with the observations and SODA results. Along the west coast of India, the West India Coastal Current (WICC) simulated by the sigma coordinate model flows polewards with an average speed of 20 cm/s. The WICC is not well represented in the SODA because of the coarse resolution near the coast. SODA uses GFDL's Z-co-ordinate model for the simulation and hence the shallow regions near the coastline are not modeled accurately. The state of art sigma coordinate ocean model is independent of the local depth and hence can be used to model both shallow shelf and deep oceanic regions. The simulation model (sigma coordinate) reproduced the WICC more accurately and more realistically as compared to SODA. There are not much significant differences in the current pattern between the surface and 50 m. depth, the only difference being that the magnitude of currents at 50 m. depth is slightly less as compared to surface level (Fig. 4.4). At 150 m. depth, strong northward flow with strength of approximately 40



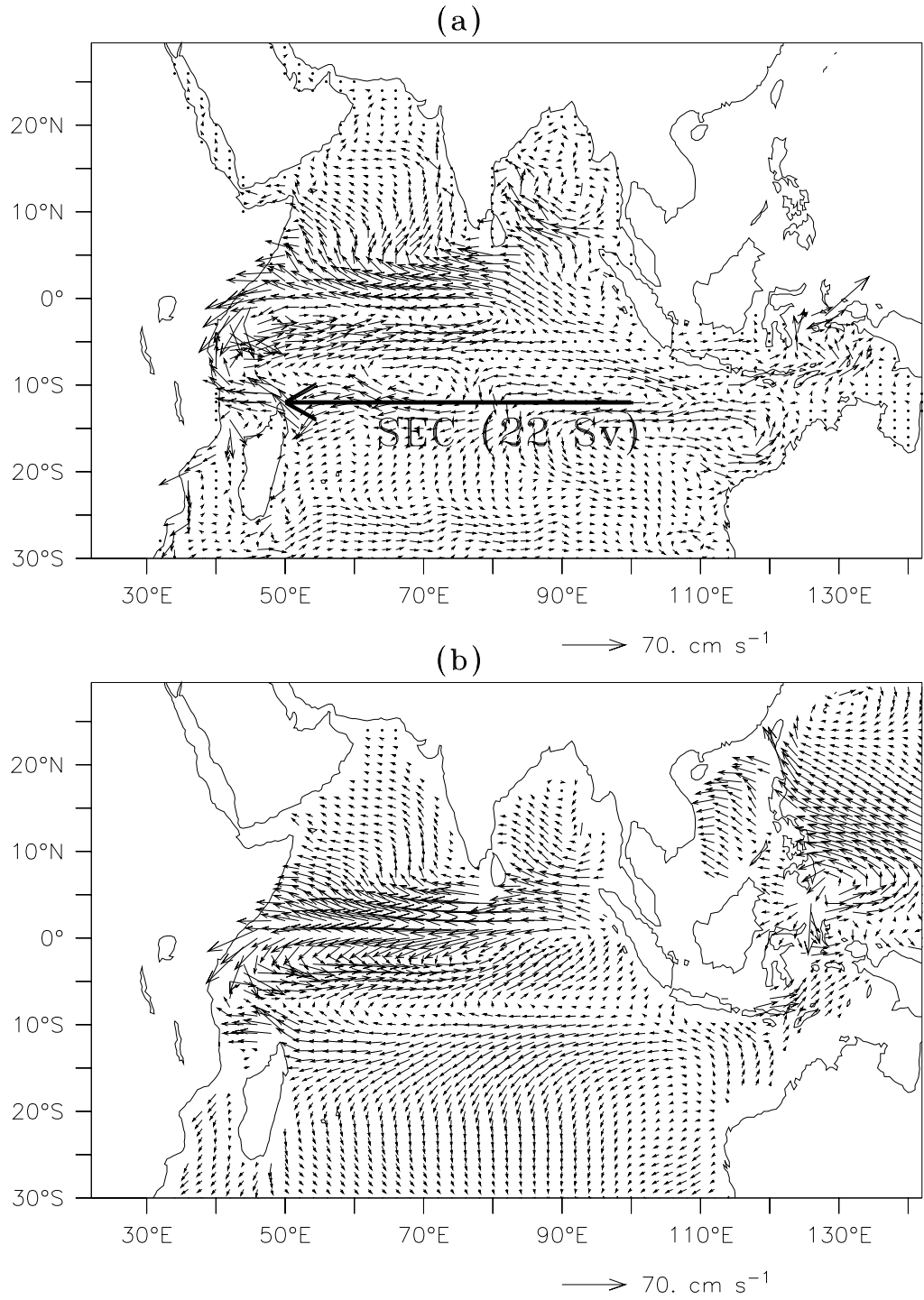
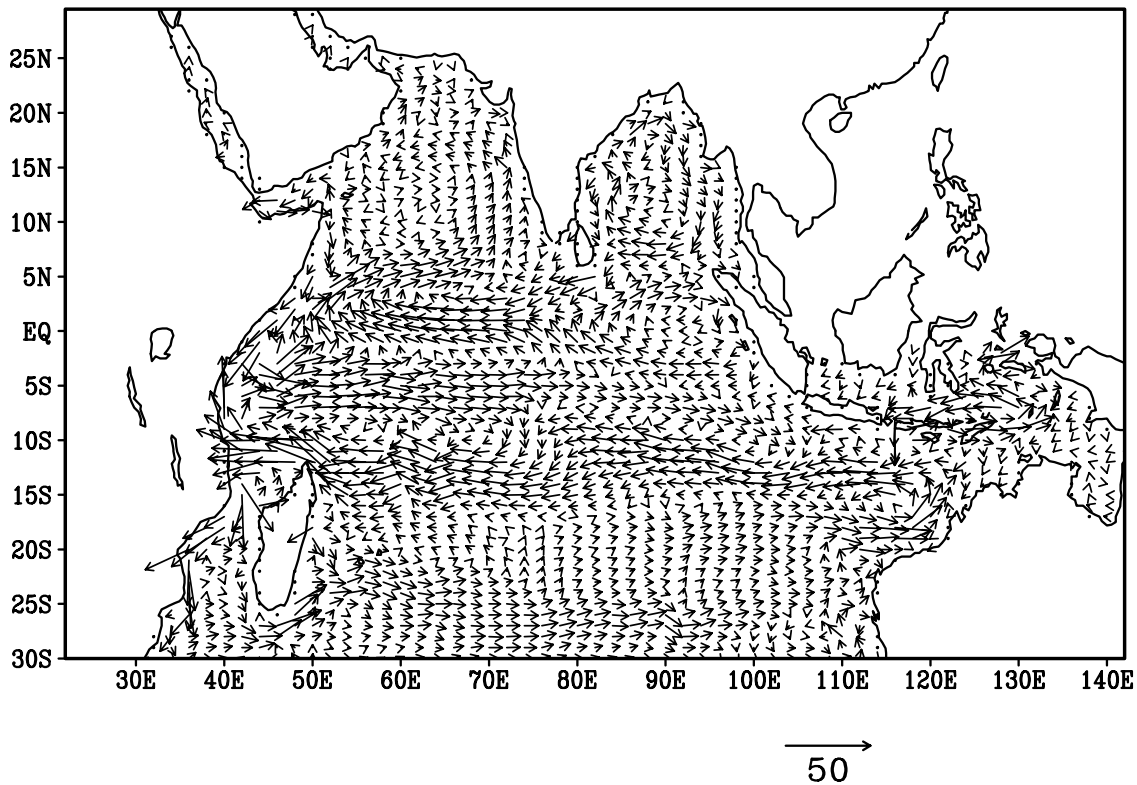


Fig.4.3. Surface velocity fields (cm/s) for January  
Model (upper panel) SODA (lower panel)

(a)



(b)

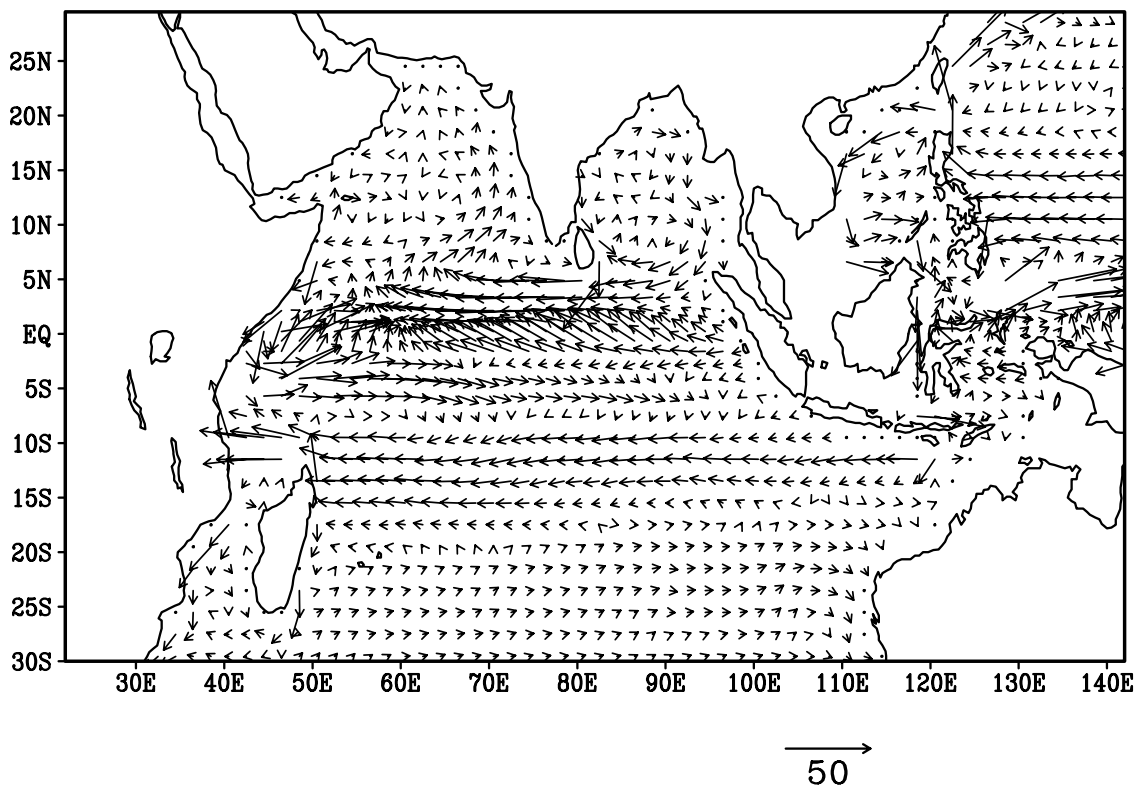


Fig.4.4. Velocity fields (cm/s) for January at 50 m  
Model (upper panel) SODA (lower panel)

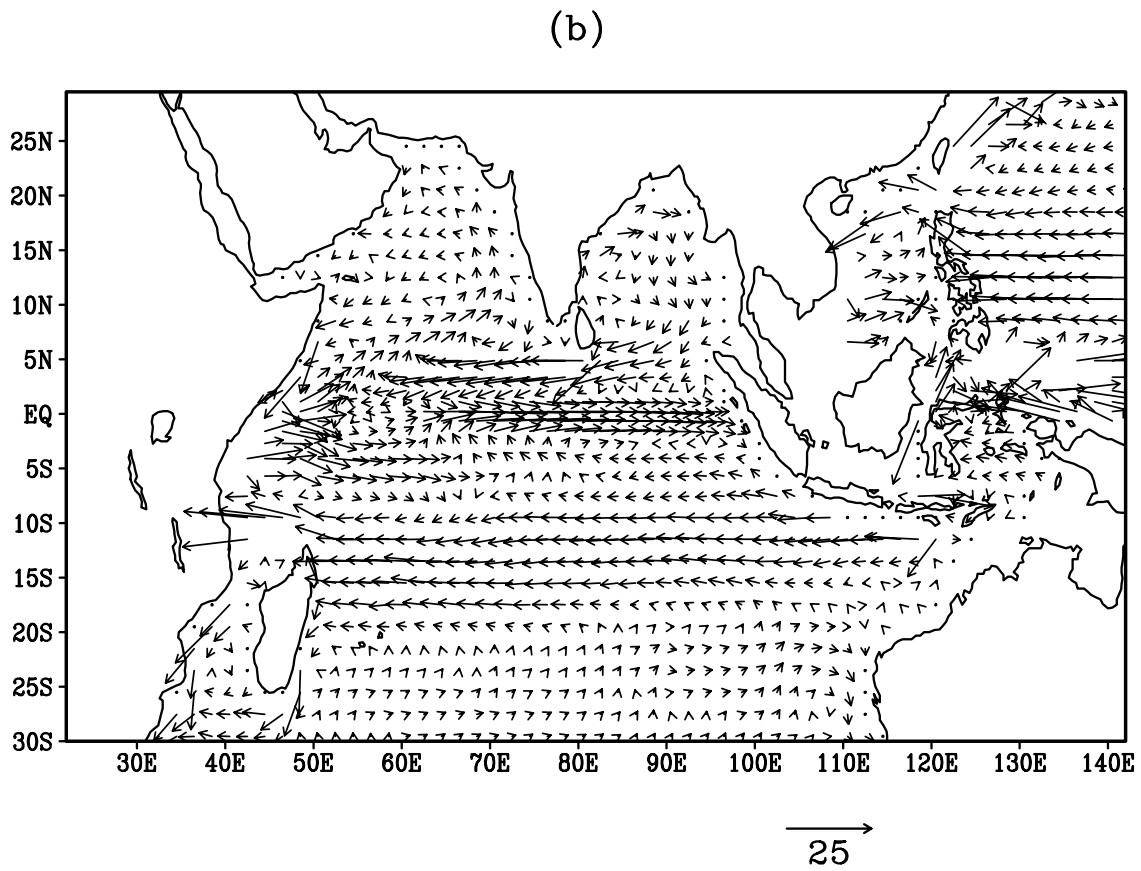
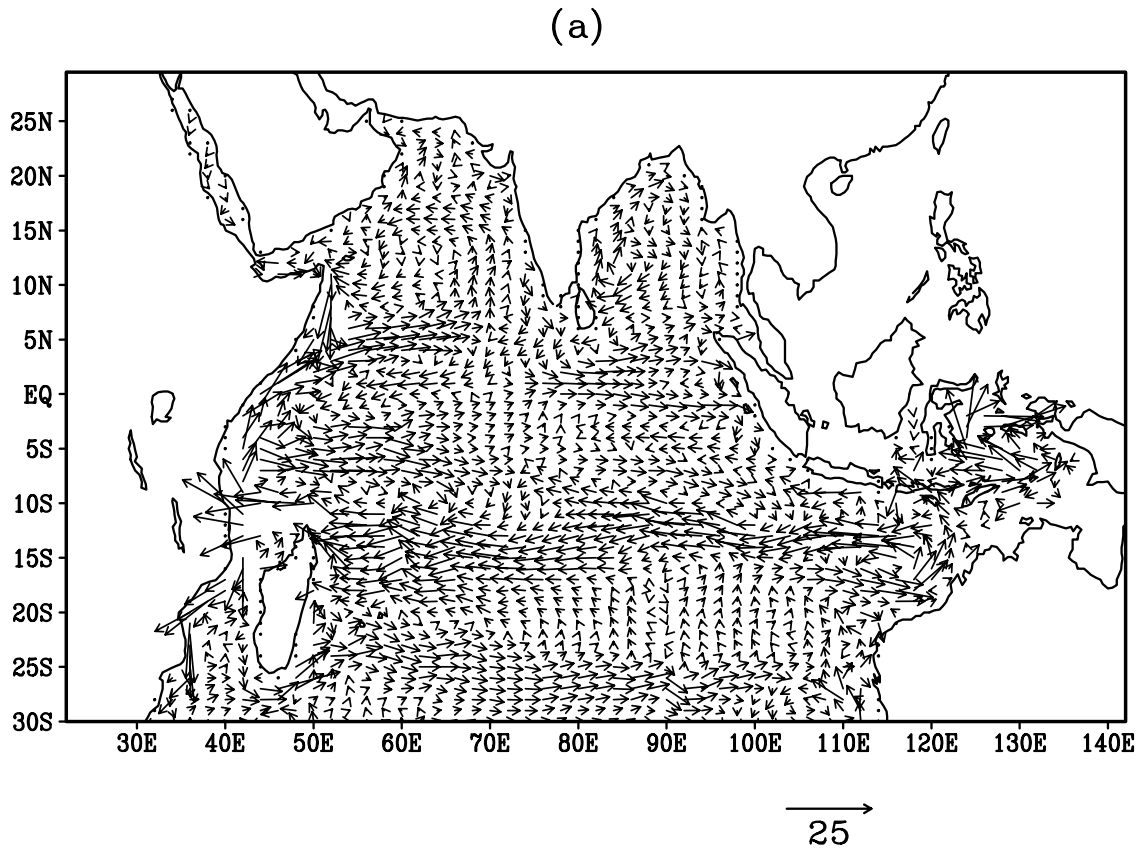


Fig.4.5. Velocity fields (cm/s) for January at 150 m  
Model (upper panel) SODA (lower panel)

cm/s is observed under the southward surface flow. The Somali undercurrent simulated by the model matches well with SODA.

To the south, the South Equatorial Current (SEC) flows between 12°S and 18°S with a speed of 45 cm/s and has a volume transport of 22 Sv across 54°E which is represented schematically in Fig. 4.5 .

### **(b) Circulation during July**

During July, the striking feature is the appearance of stronger northward flowing SC and its gyres in the western Arabian Sea. The circulation includes two eddies, which occasionally coalesce toward the end of the monsoon season (Brown et al, 1980; Swallow et al, 1983) . An intense upwelling occurs along the coast, and the two eddies advect cold low salinity upwelled water offshore. The evolution of the wind pattern during the southwest monsoon season is largely responsible for the existence of these eddies. In the simulation model, SC appears as a strong narrow current with speed up to 180 cm/s (Fig. 4.6). Both the gyres in the SC system were well reproduced by the simulation model. Compared to SODA's SC, the simulation model SC is much stronger. The volume transport of SC is 22 Sv which is in accordance with the observations. The Southwest Monsoon Current (SMC) flows as a narrow eastward current with a speed of 50 cm/s between the equator and 3°N. The SODA SMC has an approximate speed of only 20 cm/s. Westward currents exist in the equatorial region. Along the west coast of India, WICC flow equatorward with an approximate speed of 20 cm/s. At 50 m. depth, not much difference in the circulation pattern could be seen as compared to surface level (Fig. 4.7). At 150 m. depth, a weak poleward WICC undercurrent is observed in the simulation model results. WICC undercurrent in the SODA is weaker compared to simulation model results.

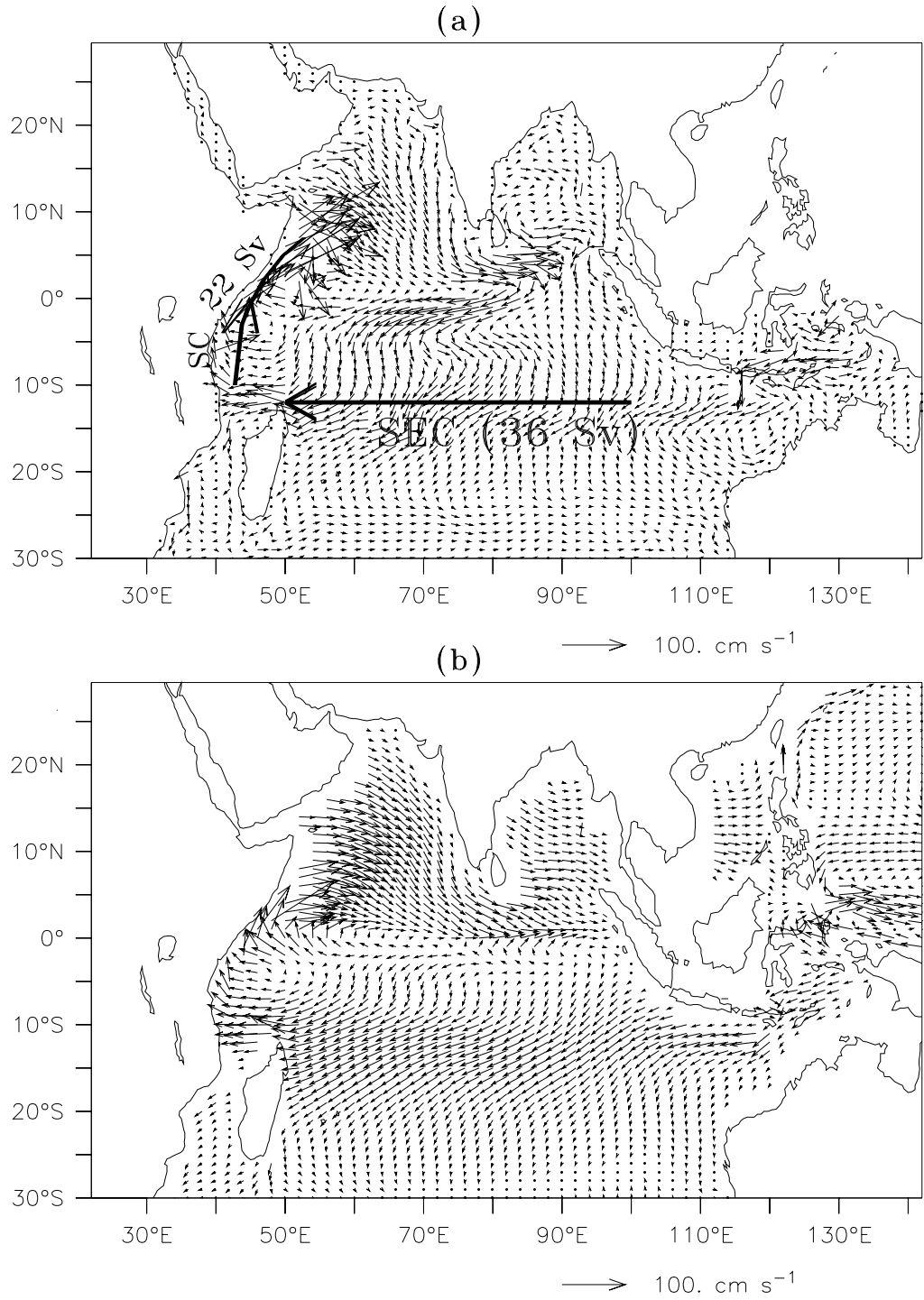


Fig.4.6. Surface velocity fields (cm/s) for July  
 Model (upper panel) SODA (lower panel)

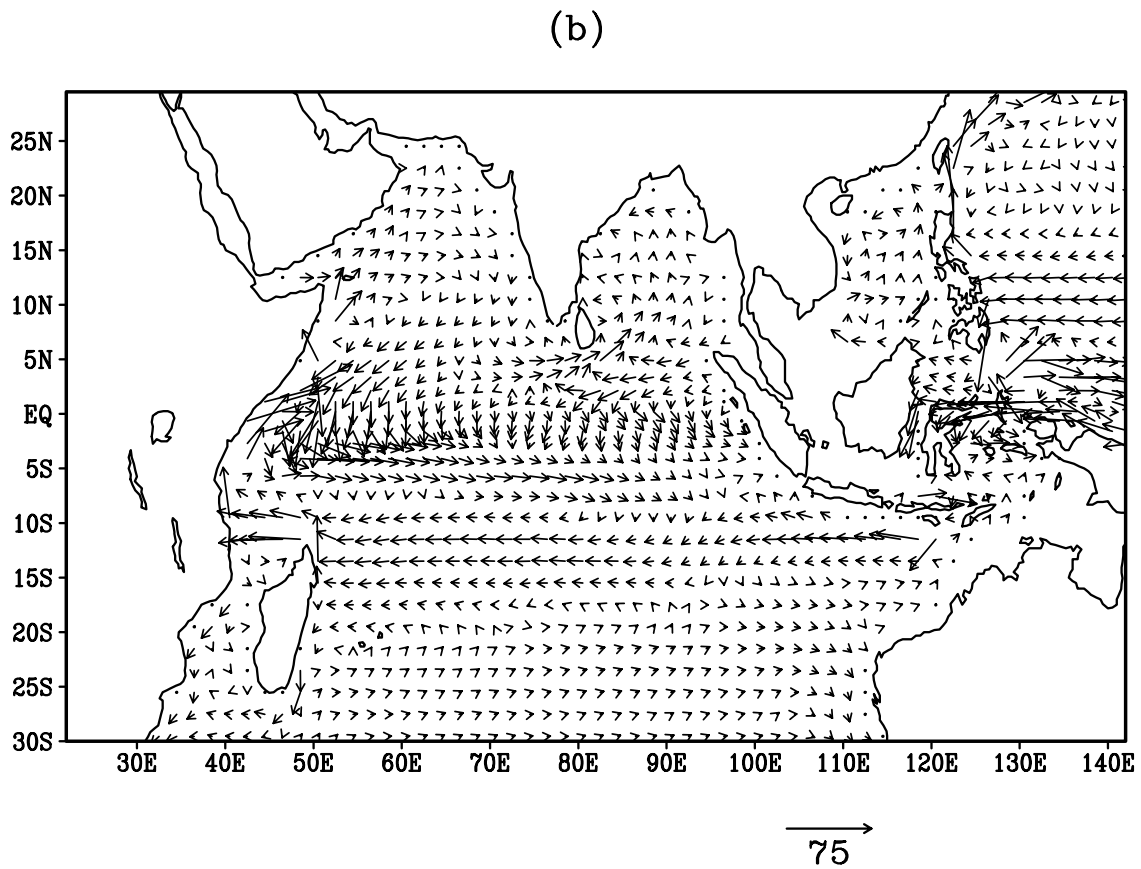
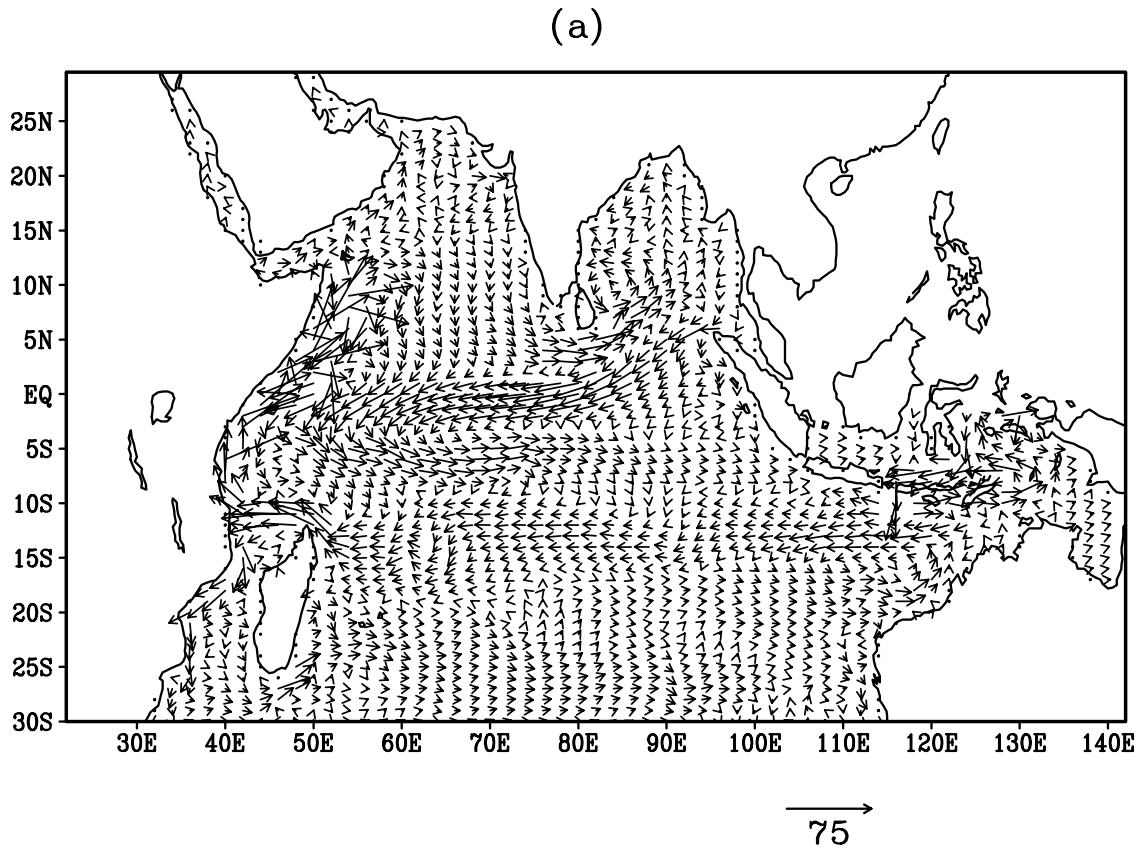
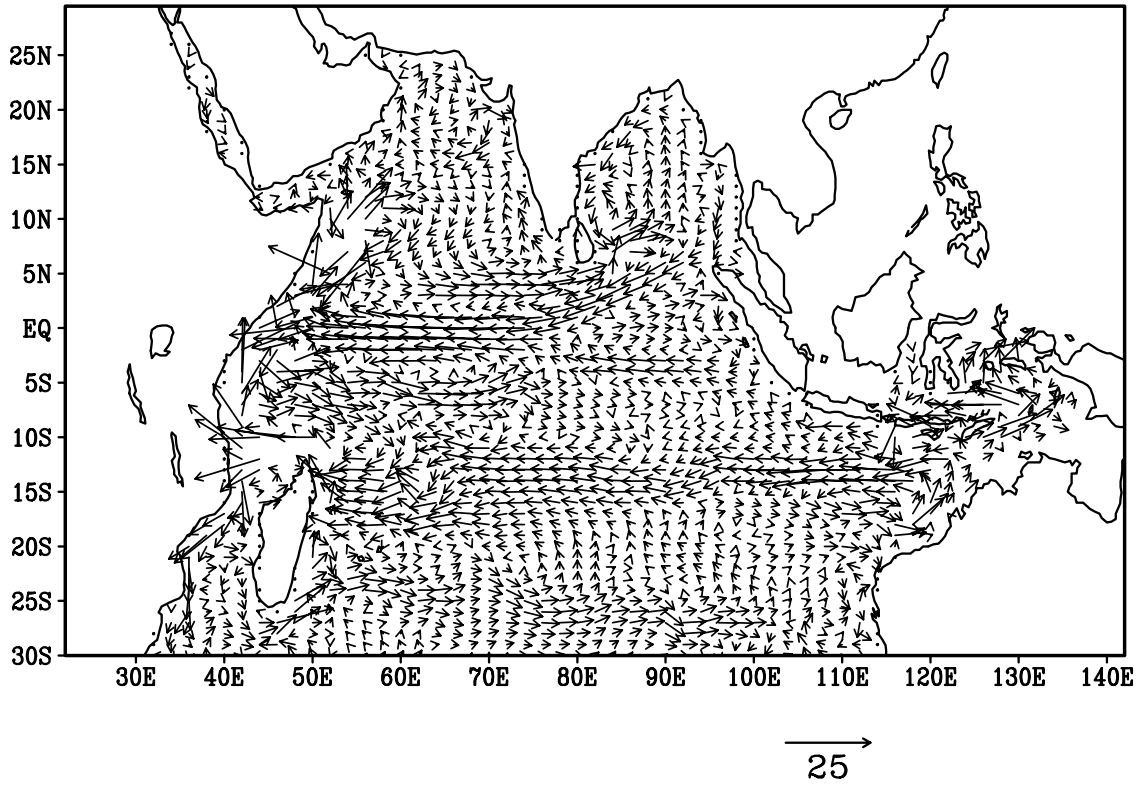


Fig.4.7. Velocity fields (cm/s) for July at 50 m  
 Model (upper panel) SODA (lower panel)

(a)



(b)

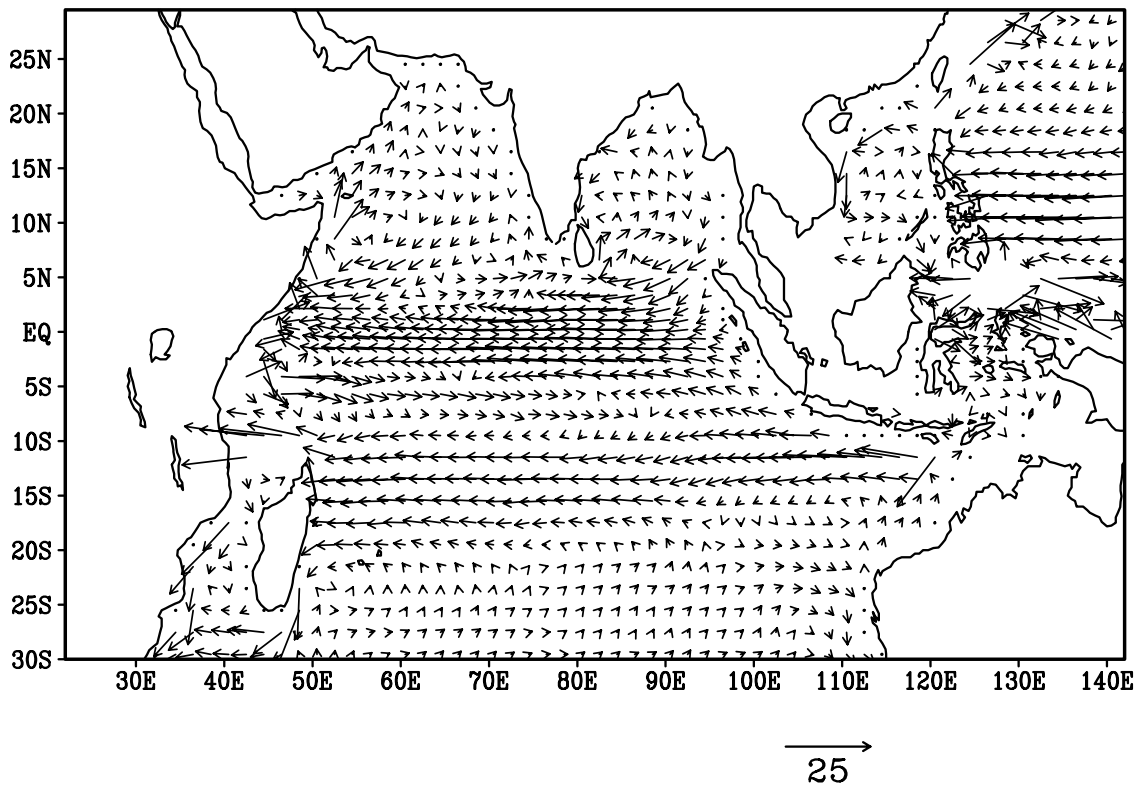


Fig.4.8. Velocity fields (cm/s) for July at 150 m  
Model (upper panel) SODA (lower panel)

In the southern Indian Ocean, the SEC appears as a zonal current with a maximum speed of 35cm/s both in the model and the SODA results. The SEC transports 36 SV across 54°E section.

### **( c ) Circulation during transition Season (April and October)**

The prominent feature of circulation in the equatorial band during both April and October (Fig. 4.9 and 4.11) is the appearance of semi-annual eastward current. These are called Wyrtki Jet (WJ). The simulation model WJ has a strength of 70 cm/s and exist in the equatorial band between 1°N and 2°S. The model WJ is comparable to SODA Wyrtki Jet both in magnitude and horizontal extent.

In the Bay of Bengal, the circulation is well developed during April. The EICC, which is the western boundary current of the subtropical anticyclonic gyre, is well reproduced in both simulation model and SODA (Fig. 4.9). The WICC flows northeastward all along the east coast of India in the simulation model results. At 50 and 150 m. depths also, the northeastward flowing WICC is well reproduced by both the simulation model and SODA during April, the EICC reverses direction in October and flows southwestward during October. The southwestward flow could be seen from surface to 150 m. depth in October (Fig 4.12-4.14).

### **4.4.2 Dynamics of large-scale circulation in the Indian Ocean**

The circulation at any point in the sea is determined by both local forcing and remote forcing whose signals are carried by the equatorial and coastal waves. The local forcing is defined to be the direct driving by the alongshore component of coastal winds and the variation in the internal density field. Remote forcing includes offshore winds that excite baroclinic Rossby waves and the equatorially trapped and coastal Kelvin waves. The circulation at any point is also influenced by circulation changes elsewhere, which are also considered as remote forcings. The equatorial



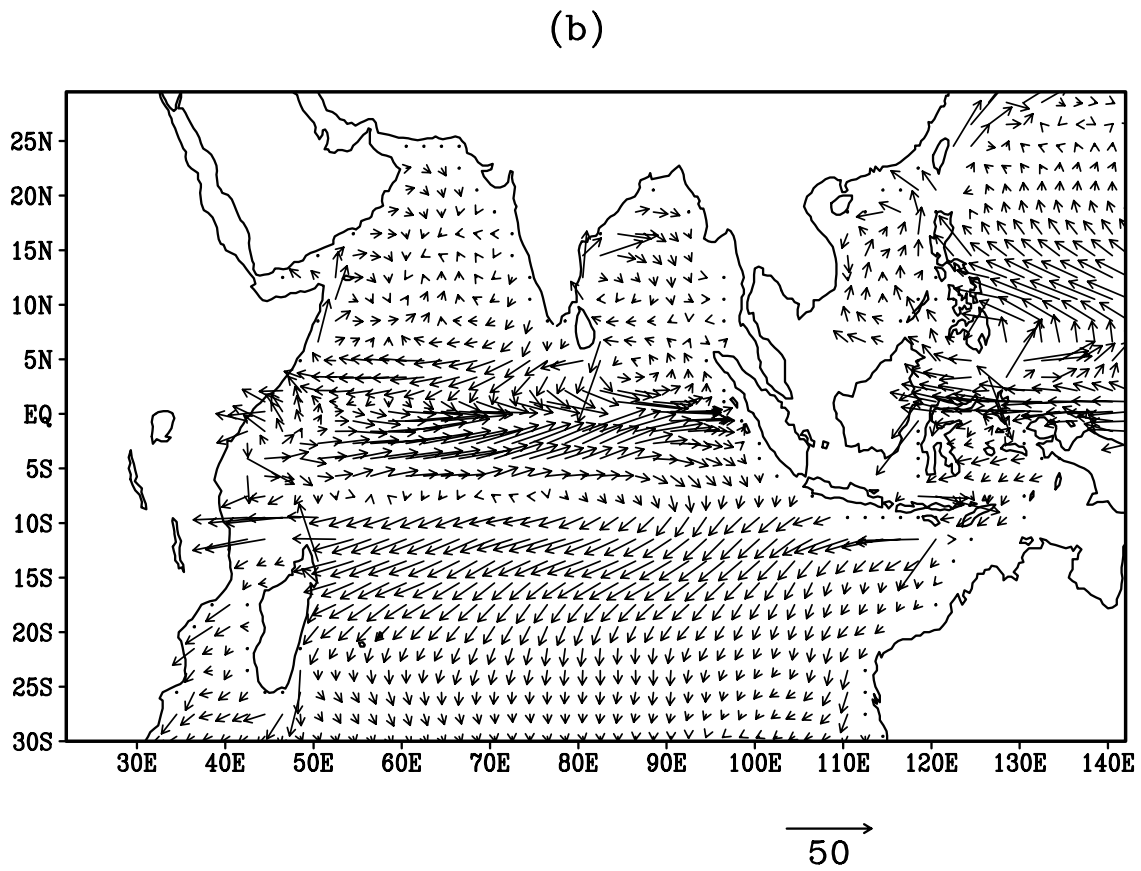
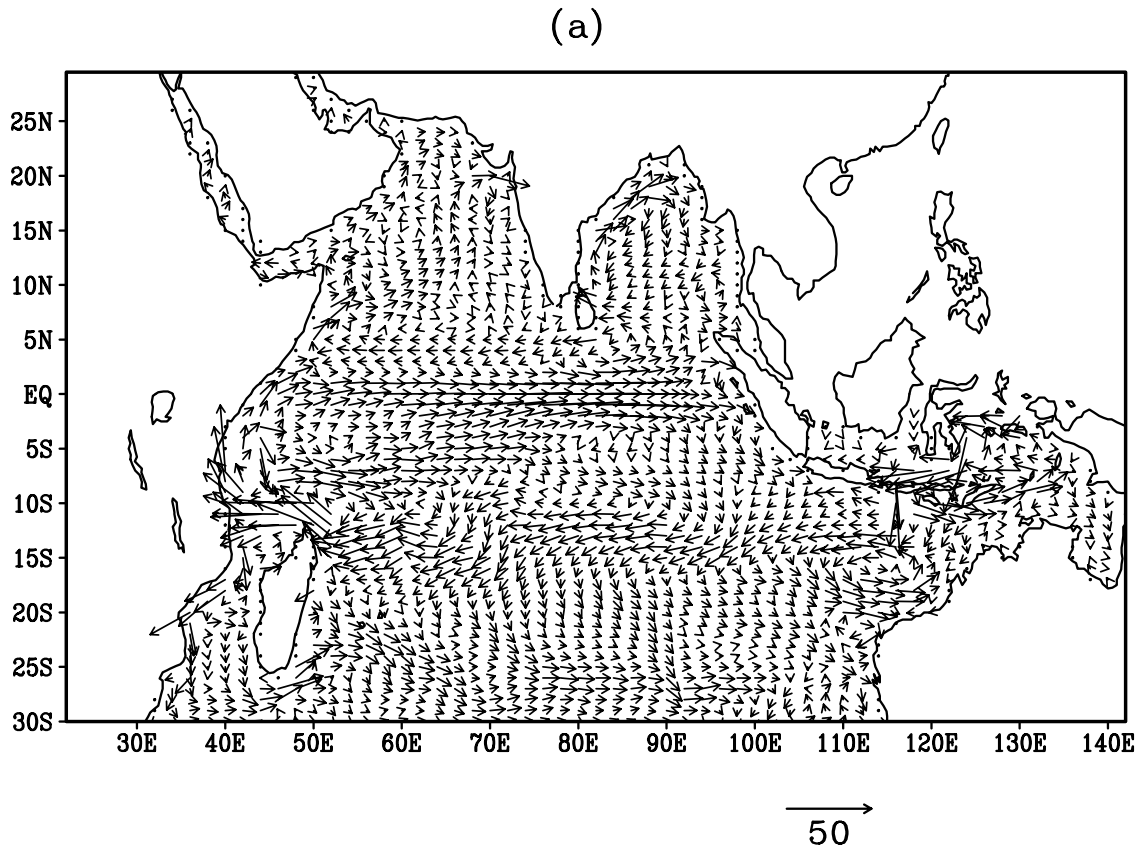
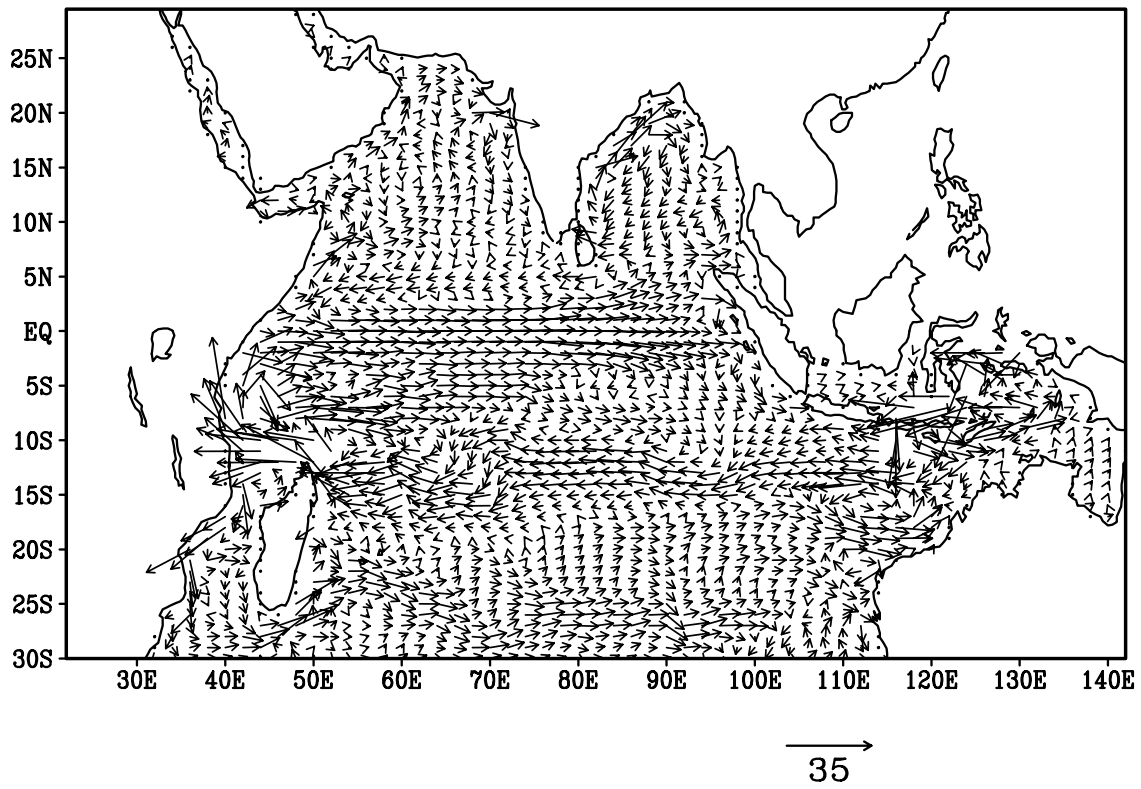


Fig.4.9. Surface velocity fields (cm/s) for April  
Model (upper panel) SODA (lower panel)

(a)



(b)

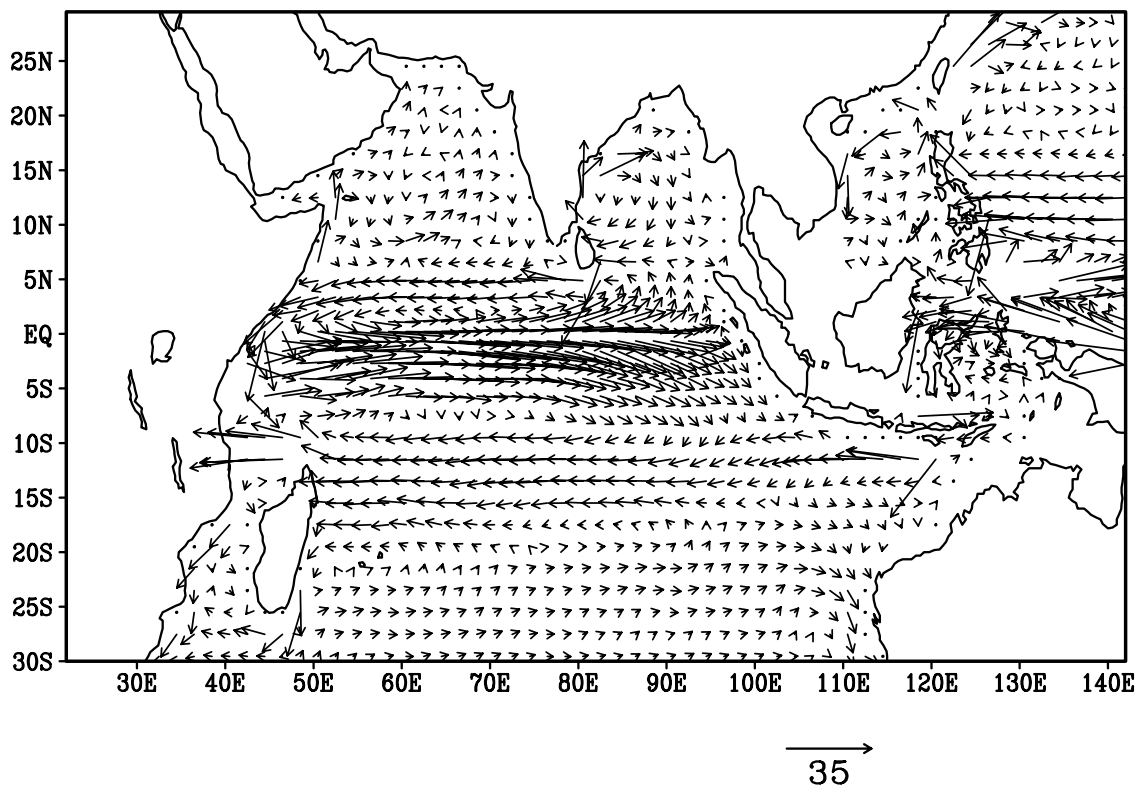


Fig.4.10. Velocity fields (cm/s) for April at 50 m  
Model (upper panel) SODA (lower panel)

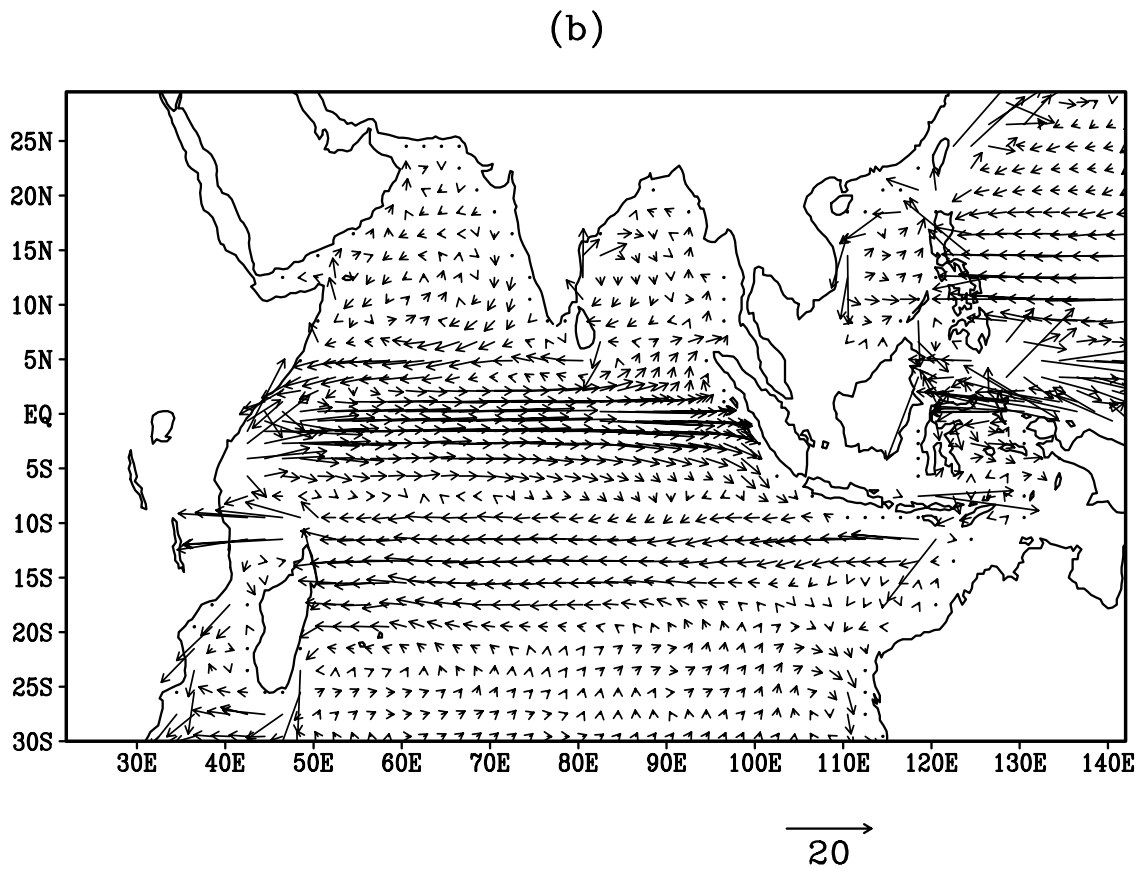
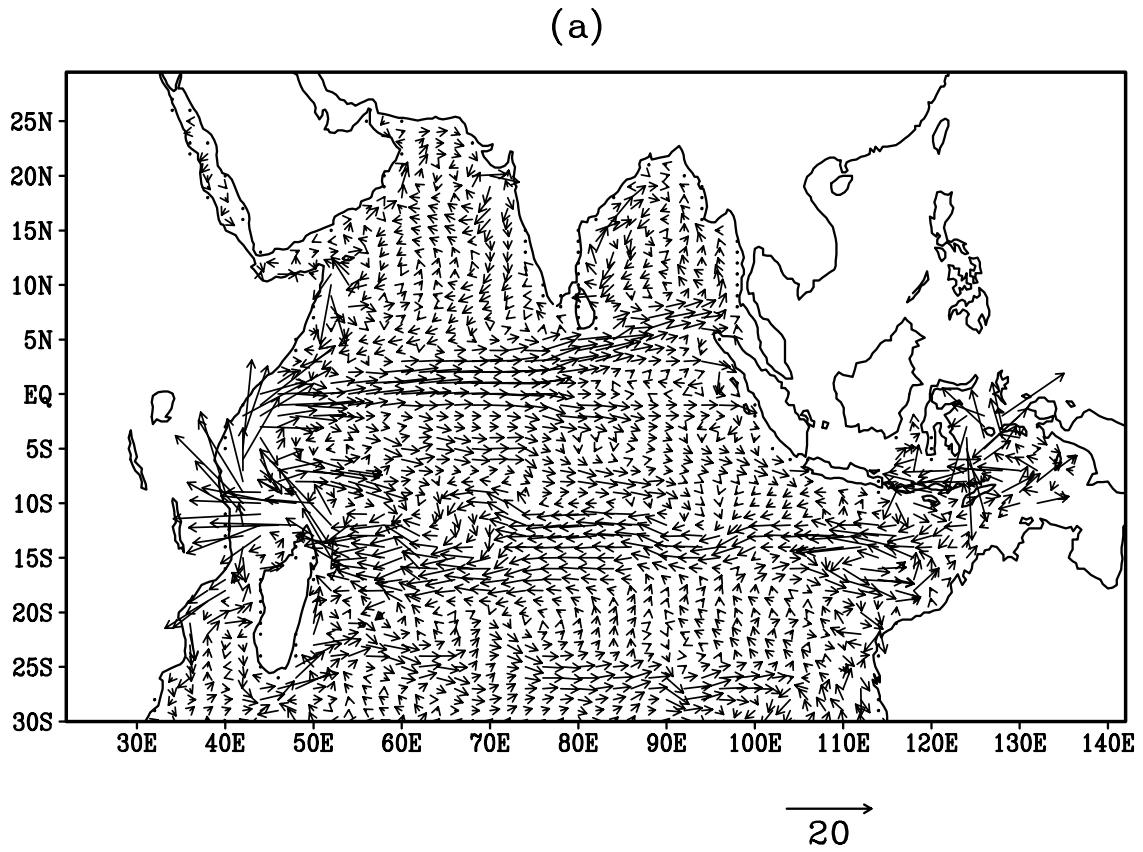


Fig.4.11. Velocity fields (cm/s) for April at 150 m  
Model (upper panel) SODA (lower panel)

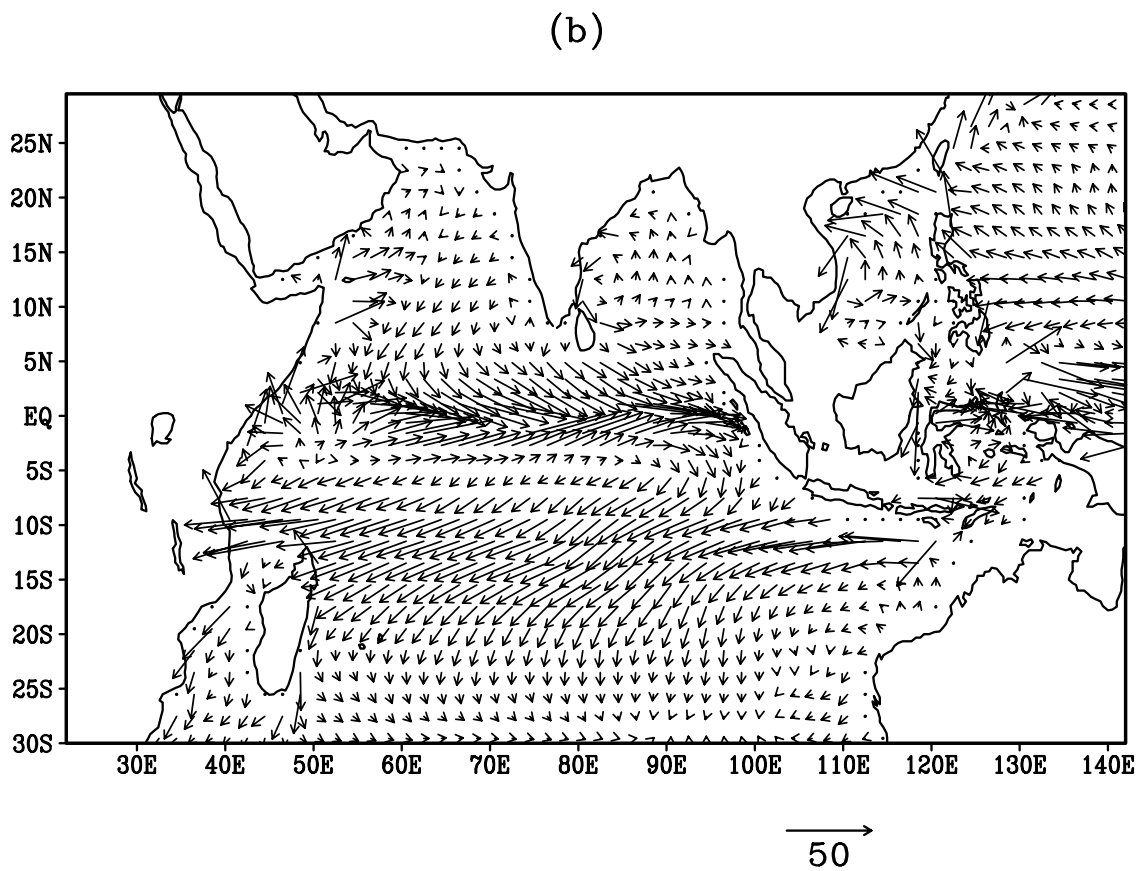
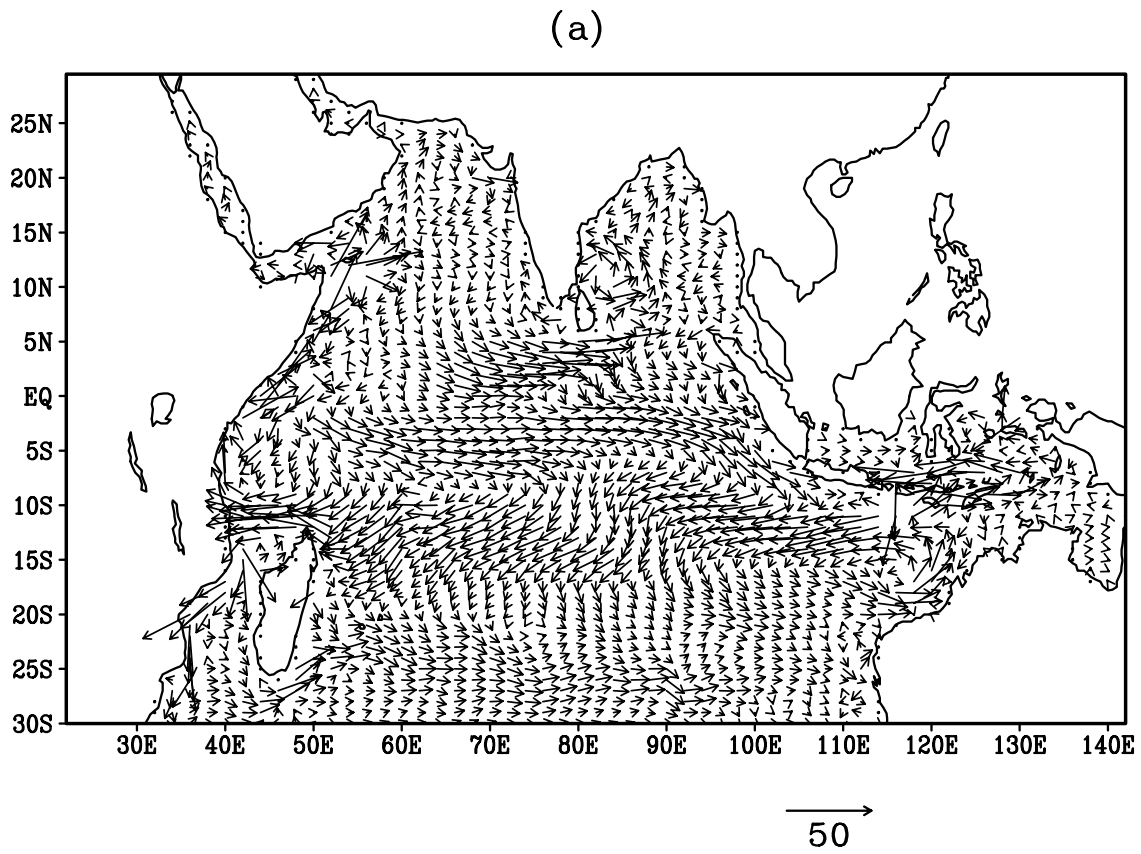


Fig.4.12. Surface velocity fields (cm/s) for October  
Model (upper panel) SODA (lower panel)

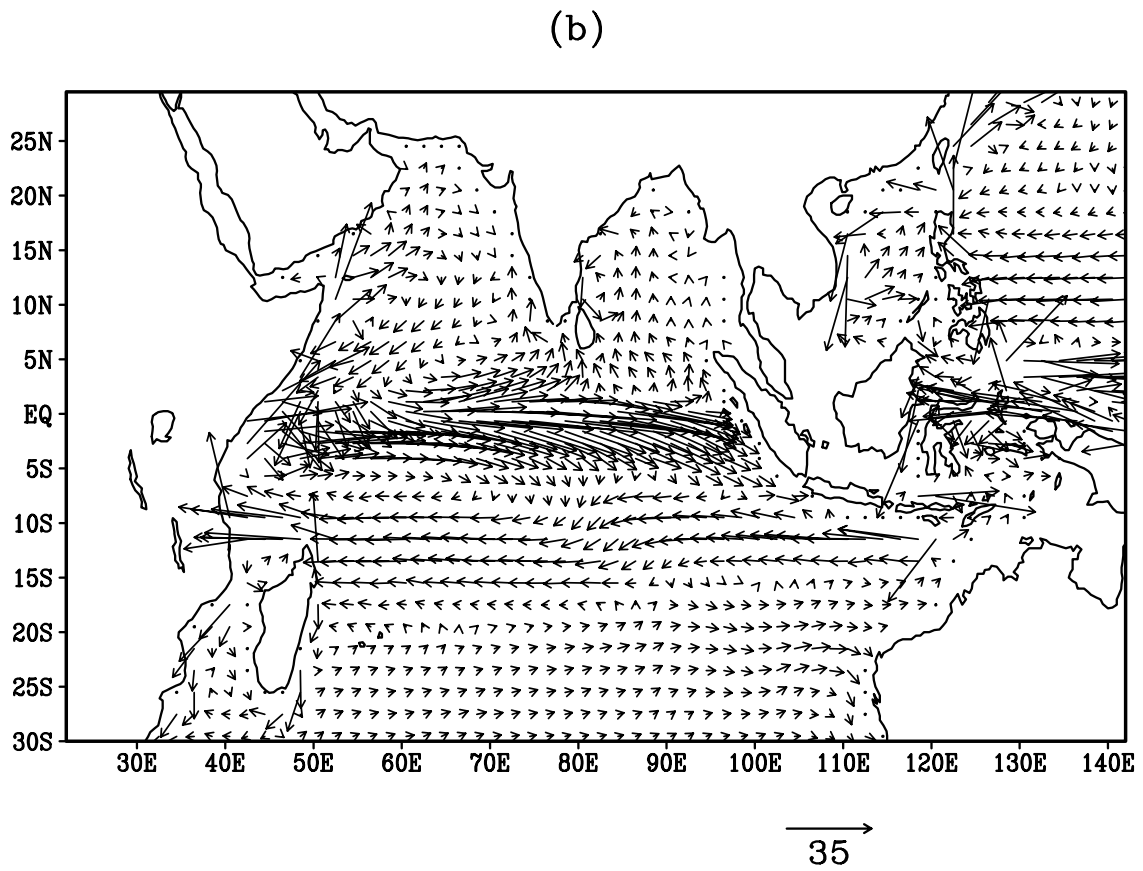
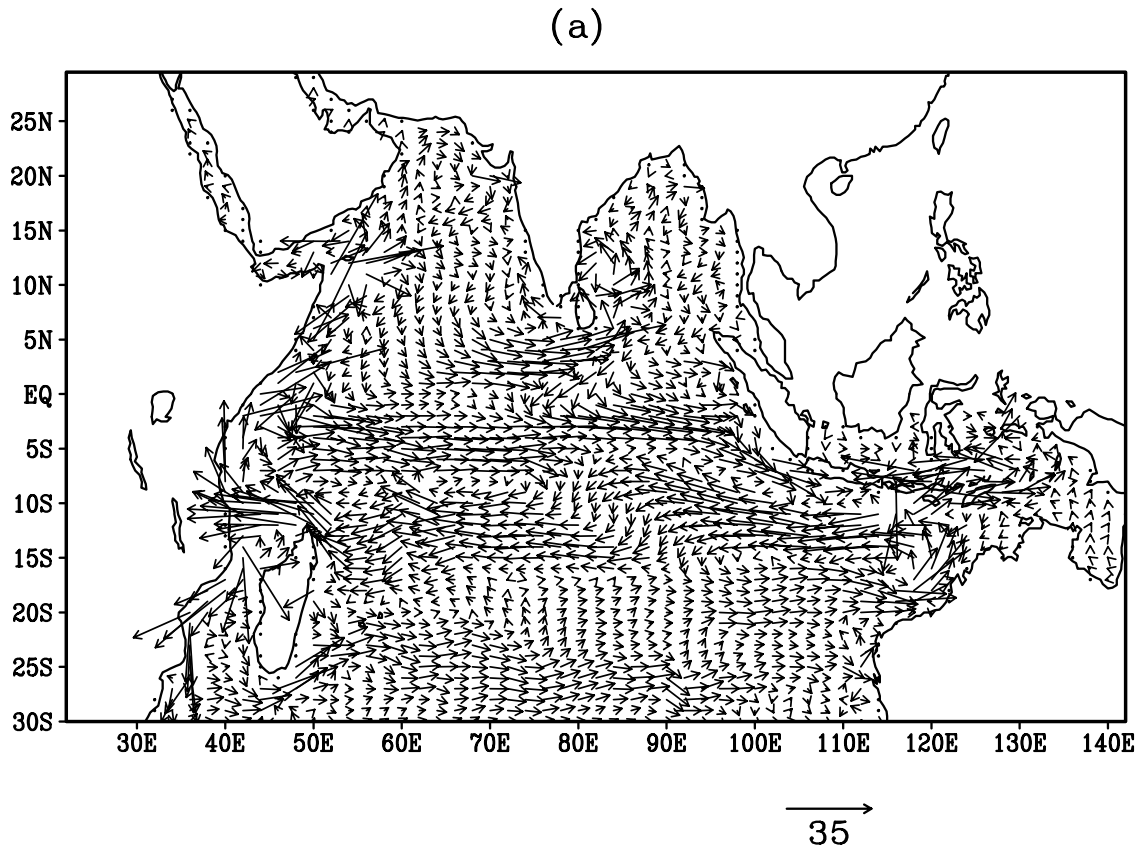
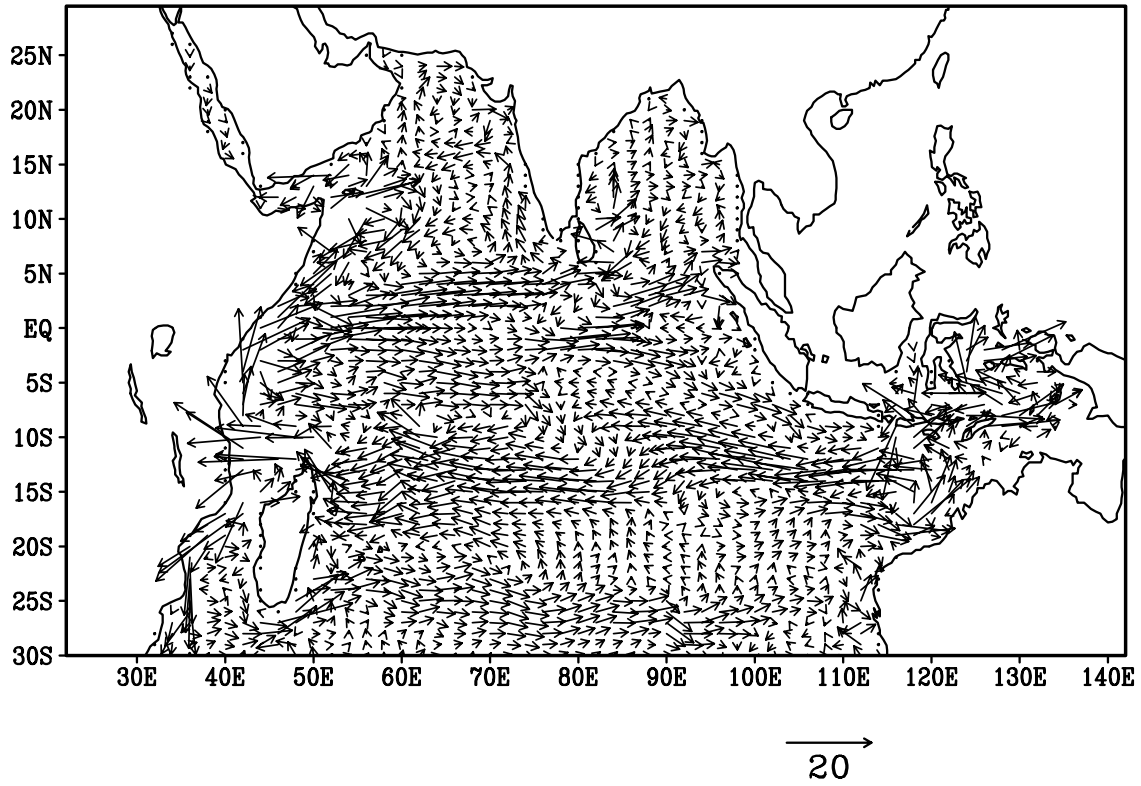


Fig.4.13. Velocity fields (cm/s) for October at 50 m  
Model (upper panel) SODA (lower panel)

(a)



(b)

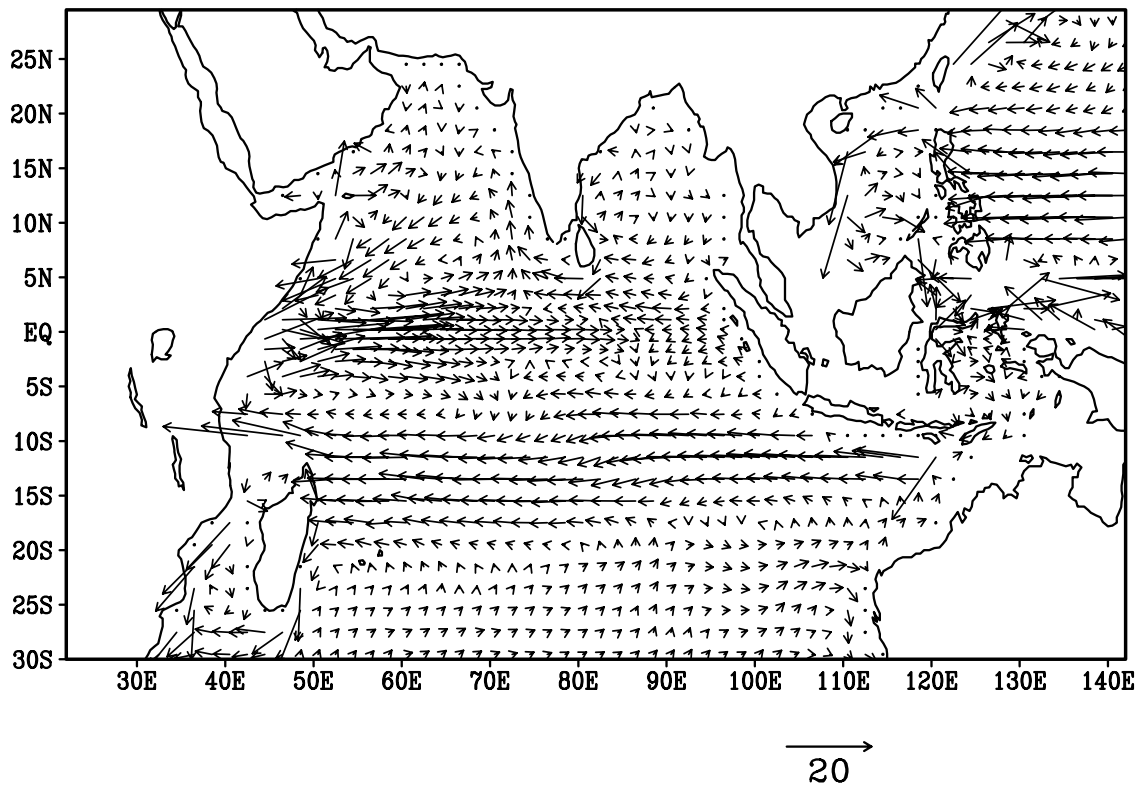


Fig.4.14. Velocity fields (cm/s) for october at 150 m  
Model (upper panel) SODA (lower panel)

Kelvin waves propagate eastwards along the equator with a speed of 2m/s and is trapped within 2.5° of equator. The equatorial Rossby waves propagate westwards with a speed of approximately 0.5 m/s and the speed decreases with increase in latitude. The coastal Kelvin waves propagate with a speed of approximately 2 m/s with the coast on its right side in the northern hemisphere.

The role of each of these forcing on the circulation of the Indian Ocean is examined by comparing the state of art simulation model results with the semi-diagnostic (adaptation) model results. The semi-diagnostic model being forced with steady forcing of wind and density field and since the model attains quasi-steady state within a short period of time (2-3 months), the effect of long waves cannot be obtained in the model solutions. So comparing these two model solutions will reveal the role of each of these forcing on the circulation of the Indian Ocean.

The surface circulation from the semi-diagnostic and simulation model along with SODA simulation is presented in Fig. 4.15 to 4.18. Though the overall magnitude of various current systems from the simulation and semi-diagnostic model matches well and compares with the results from SODA, there are variations in the intensity of the current systems between the models. The simulation model results are in agreement with SODA simulation. But semi-diagnostic current systems show variation in the intensity of various current systems. The difference in intensity is observed for WICC, NMC and SMC in the Arabian Sea. The WICC is weaker in the semi-diagnostic computations during January than the simulation results. The monsoon currents are weaker in semi-diagnostic results than in simulation results. In the equatorial region, considerable difference in the strength of EJ's is observed between the models during the transition seasons. Since the intensity of wind field is considerably reduced during the transition season, the flow field is dominated by the remote forcing and the internal density field. The remote forcing is absent

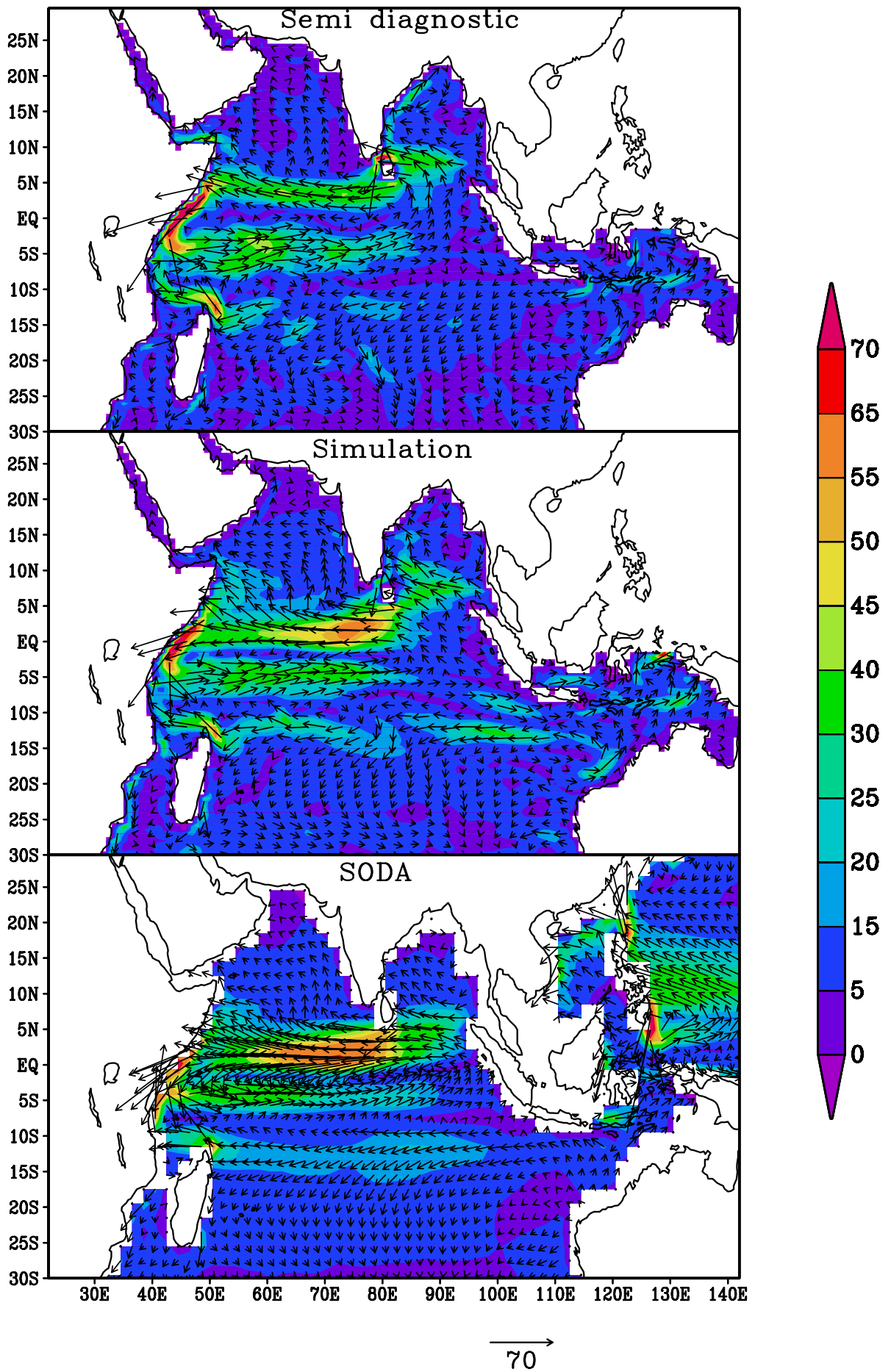


Fig.4.15. Surface velocity fields (cm/s) for January



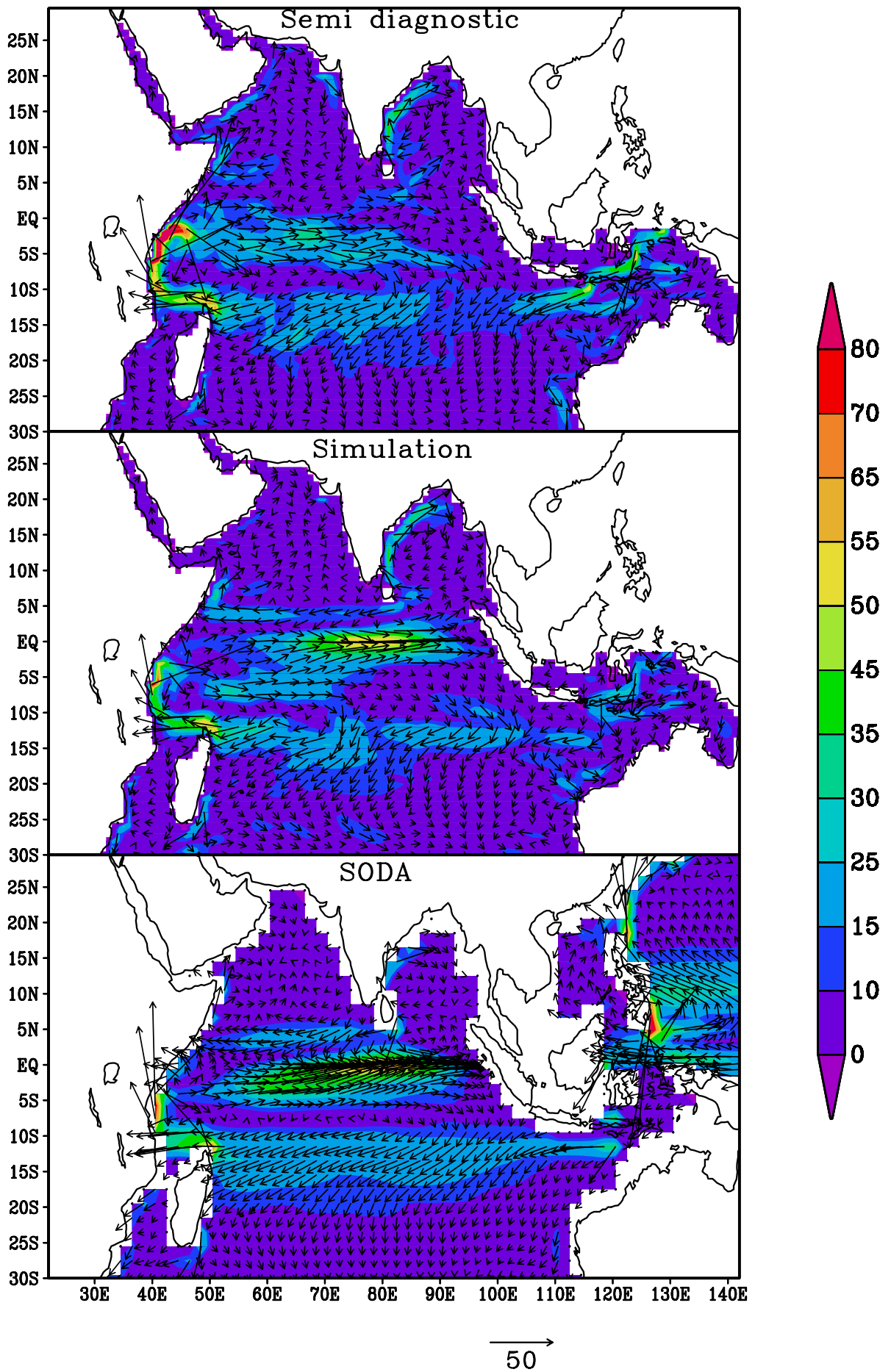


Fig. 4. 16. Surface velocity fields (cm/s) for April

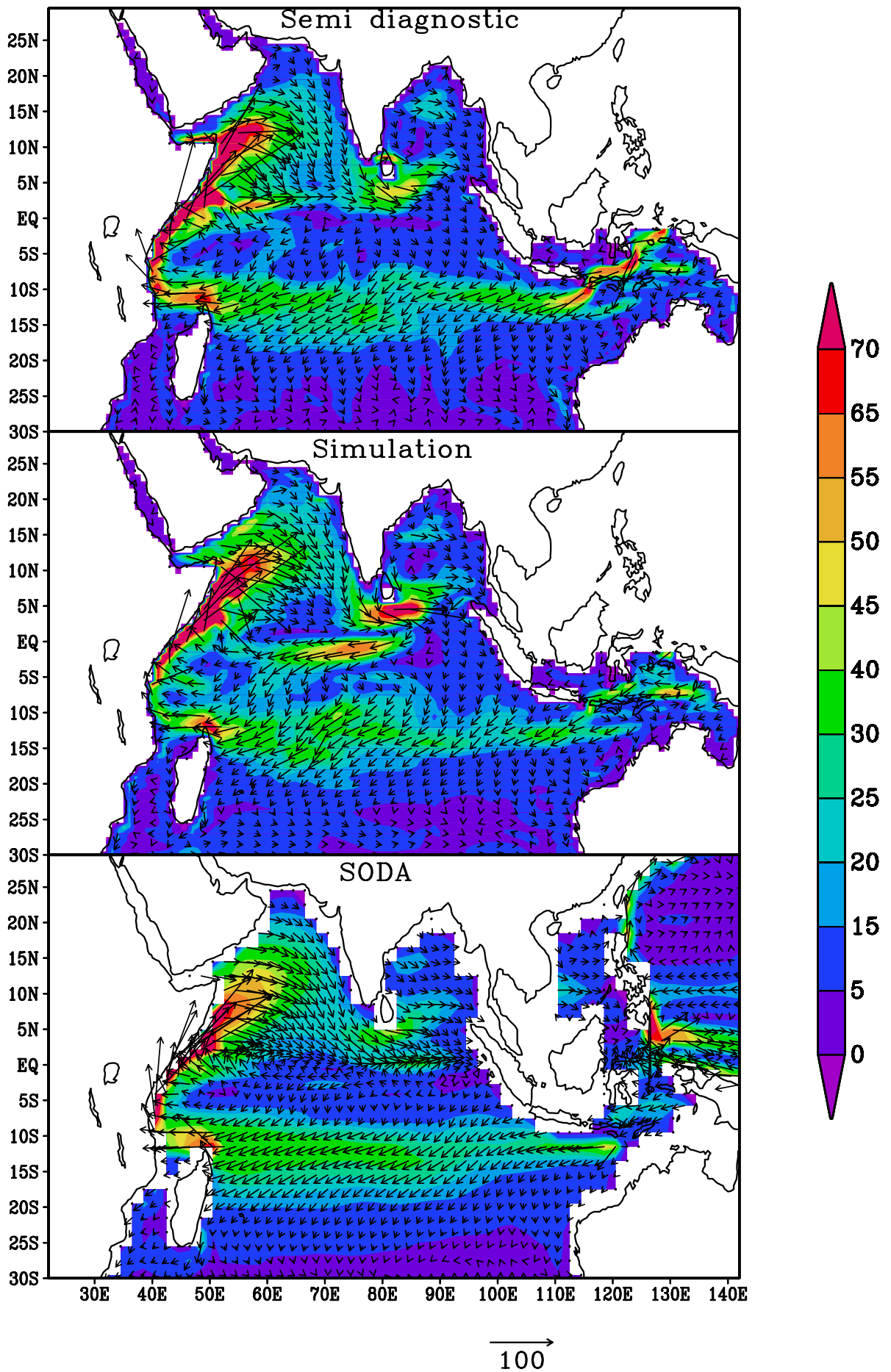


Fig. 4.17. Surface velocity fields (cm/s) for July

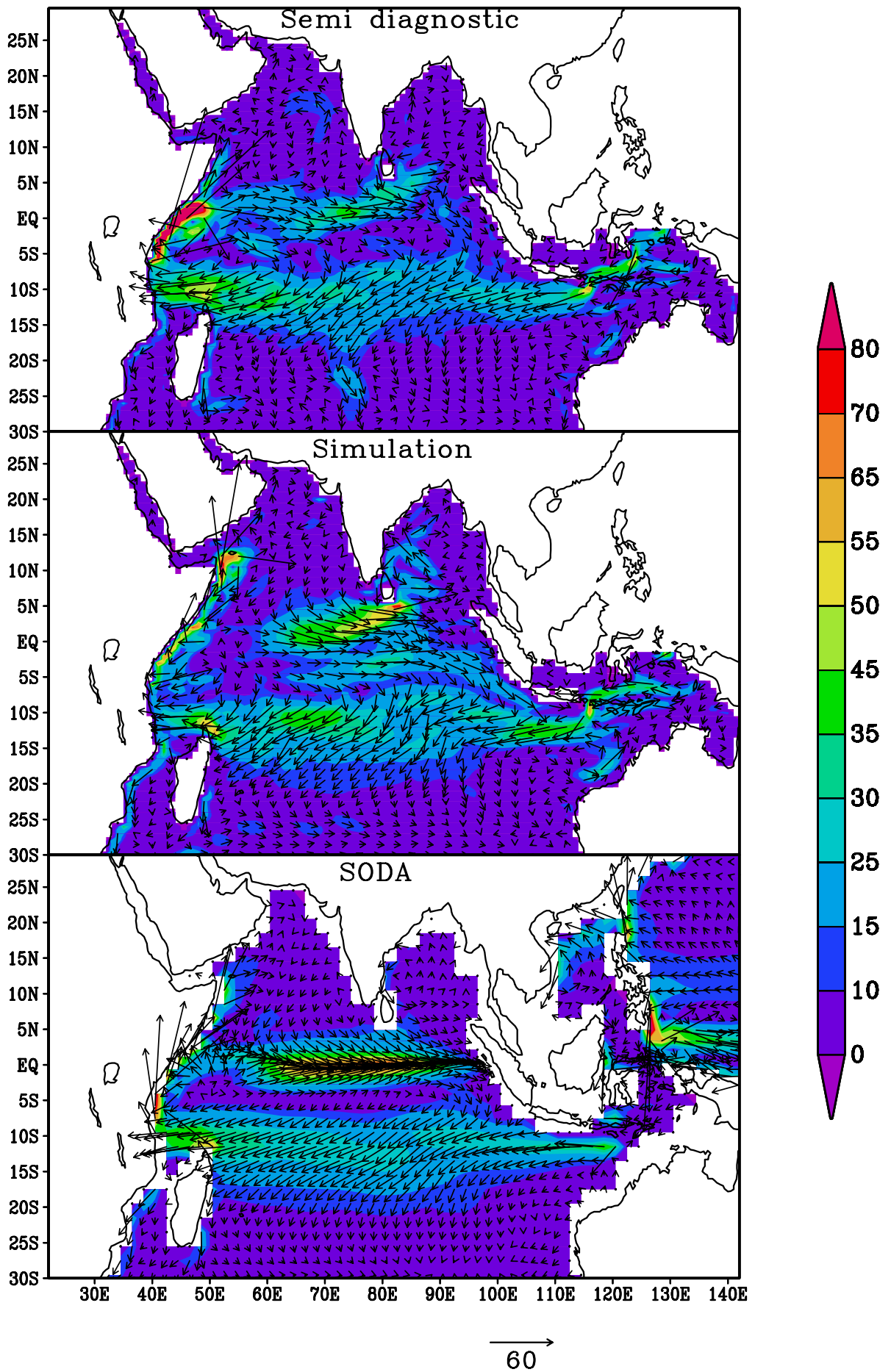


Fig. 4.18. Surface velocity fields (cm/s) for October

in the semi-diagnostic integration and hence the EJ's are weaker in semi-diagnostic computation. In the Bay of Bengal, the two model simulations show difference in the strength of EICC during the peak phase of southwest monsoon season (July), October and January. During July, the reversal of the EICC to equatorward at the southern regions is more prominent in simulation results. During October, strong EICC is reproduced in the simulation results than the semi-diagnostic computations. In the equatorial regions during July and January, eastward currents are seen in semi-diagnostic results, while westward currents exist in simulation and SODA computations.

Another difference observed between the two model simulations is in the deeper levels. The circulation features reproduced by the semi-diagnostic model matches with simulation results in the upper levels. The circulation below 200 m is not realistically reproduced by the semi-diagnostic model. This may be due to the lack of long term integrations in the semi-diagnostic model for the evolution of circulation at deeper levels.

The major surface current systems are realistically reproduced by both semi-diagnostic and simulation models. Hence the variation in the magnitude of various current systems between the two models may be due to the difference in the forcing mechanisms of these models. The remote forcing is absent in the semi-diagnostic computation, the current systems which are remotely forced show variation in strength. In the northern Indian Ocean, the influence of the remote forcing is evident in WICC, EICC, Monsoon Currents and Equatorial Jets as discussed earlier. The equatorial winds have been shown to be important forcing mechanism for these currents (Mc Creary et al., 1993, 1996). The equatorial westerlies over the Indian Ocean mainly during the transitions generate eastward propagating Kelvin waves, which on reflection from the coast of Sumatra, excite westward propagating Rossby waves and coastal Kelvin waves that propagate poleward towards the Bay of Bengal in the north and

along the Indonesian Islands in the south (Clark and Lui, 1993, Mc Creary et al ., 1993, Sprintall, 2000).

The winds along the western boundary of the Bay of Bengal are southwesterly during summer monsoon and northeasterly during the winter monsoon. The SW-NE alignment of the coast makes the wind stress parallel to the coast and EICC follows the wind field. Both in the simulation and semi-diagnostic model calculations, EICC is of nearly the same strength and follow the direction of the winds during the monsoon seasons. The maximum strength of EICC is observed during March and November. The peak months of the monsoons (January and July) do not coincide with the times of maximum current speed of EICC. So the local alongshore winds alone can not drive the EICC. This is evident from the model simulations in which, EICC is reproduced both in the simulation and the semi-diagnostic integrations. But the magnitude of EICC is more during the transition seasons in the simulation model. This clearly shows that remote forcing effects do contribute to EICC.

Along the west coast of India, the WICC flows equatorward during the SW monsoon season and poleward during the northeast monsoon season which is against the prevailing wind direction during winter. Hence the winter WICC is not completely forced locally by the wind. The coastal Kelvin waves forced by the winds along the east coast of India bend around Sri Lanka to propagate poleward along the west coast forming the winter WICC. The semi-diagnostic model shows a weak poleward WICC of magnitude 5 cm/s, whereas in the simulation model, WICC is strong and attains a maximum speed of 25 cm/s. It appears as strong narrow current all along the west coast of India extending from 6.5°N in the south to 25°N in the north. The propagation of coastal Kelvin waves from the western Bay of Bengal to the eastern Arabian Sea is possible because the sum of the e-folding scale of coastal Kelvin waves south of Sri Lanka (~2.25°) and equatorial Kelvin waves (~2.5°) is less than the distance between the



southern tip of Sri Lanka and the equator ( $6^\circ$ ), (Shankar et al., 2002). This allows the Kelvin waves from the Bay of Bengal to pass into the Arabian Sea making the eastern boundary of the Arabian Sea a continuation of the western boundary of the Bay of Bengal. A part of the energy from the coastal Kelvin wave along the southwest coast of India propagate westwards as Rossby waves.

During the southwest monsoon season, strong upwelling occurs along the west coast of India. SST's are lowered by nearly  $2^\circ\text{C}$  in both the model solutions. These are forced by strong south-westerlies over the Arabian Sea which turns around the central Arabian Sea to blow from the northwest along the west coast of India favoring coastal upwelling along the west coast of India.

In the Somali Current region, during the southwest monsoon season, both the simulation model as well as the semi-diagnostic model reproduced the Somali current and its gyres with more or less same magnitude. Hence the local alongshore wind associated with the Findlater Jet is the main driving mechanism in this region. Along the eastern side of the Findlater Jet, the wind stress curl is negative, which produces anticyclonic circulation. There are many studies which suggested that the Great Whirl of the Somali Current is directly forced response to this negative wind stress curl (Schott and Quadfasel, 1982; Luther et al., 1985, Schott et al., 2001).

The SMC appears as an extension of the SC system in the western Arabian Sea, flows towards the southeast in the eastern Arabian Sea, and then flows eastward south of India. The magnitude of SMC is  $20\text{ cm/s}$  in both model computations. The intrusion of SMC into Bay of Bengal which is caused by remote forcing effects (Vinayachandran et al., 1999) could not be captured by the model. The NMC during the winter monsoon flows

westwards with a speed of 40 cm/s in the simulation model and 30 cm/s in the adaptation model.

In the equatorial Indian Ocean during the monsoon transitions, the westerly wind drive intense eastward jets called the Wyrki Jets (WJ). The Kelvin waves associated with the Equatorial Jets propagate eastward, and on reaching the eastern boundary, one part of the energy reflects as Rossby waves and the other propagates poleward as coastal Kelvin wave. The WJ during the monsoon transition has a magnitude of nearly 80 cm/s in the state of art simulation model, but are weaker in the adaptation model.

South of the monsoon regime, ie, 10°S, the main feature of circulation is the westward flowing SEC between 8°S and 15°S. The SEC roughly follows the line of zero wind stress curl. Seasonal variability in the latitudinal range of the SEC is generated to the east of 100°E by the annual cycle in the wind stress curl and propagating westwards as the Rossby waves (Woodburry et al., 1989). The state of art simulation model SEC extends between 8°S to 15°S with a speed of 40 cm/s during the northern summer (July) and between 10°S and 6°S with a speed of 30 cm/s during the northern winter (January).

#### **4.5 Conclusions**

The state of art simulation results are compared with the results from SODA (Simple Ocean Data Assimilation, Carton et al., 2000) to validate the model. The circulation obtained from the simulation model are in agreement with the SODA results and also with available observations. All the current systems are well reproduced in the model along with their undercurrents and gyres. The volume transport for major currents were computed and compared with transport estimates available in the literature. The volume transport was also found to be comparable with the existing estimates for different currents. The dynamics of each of the

current systems are explained by comparing state of art simulation model results with the semi-diagnostic (adaptation) model results. The simulation model yields time-varying unsteady circulation of the Indian Ocean whereas the semi-diagnostic model gives the steady state circulation. Thus the role of local versus remote forcing on the computed circulation of the Indian Ocean is explained by comparison of the simulation and semi-diagnostic model results.